

Acknowledgment. We are grateful for funding from NSF Grant CHE-9115286 and NIH Grant HL-13652.

Supplementary Material Available: Tables of crystallographic data, bond distances and angles, anisotropic displacement coef-

ficients, calculated hydrogen atom coordinates, magnetic susceptibility data, and positional parameters for $[\text{Fe}(t\text{-tpchxn})](\text{ClO}_4)_2 \cdot \text{H}_2\text{O} \cdot \text{CH}_3\text{OH}$ (10 pages); a listing of observed and calculated structure factors (9 pages). Ordering information is given on any current masthead page.

High-Spin Molecules: $[\text{Mn}_{12}\text{O}_{12}(\text{O}_2\text{CR})_{16}(\text{H}_2\text{O})_4]$

Roberta Sessoli,¹ Hui-Lien Tsai,² Ann R. Schake,^{3a} Sheyi Wang,^{3a} John B. Vincent,^{3a} Kirsten Folting,^{3b} Dante Gatteschi,^{*1} George Christou,^{*3a} and David N. Hendrickson^{*2}

Contribution from the Department of Chemistry-0506, University of California at San Diego, La Jolla, California 92093-0506, Dipartimento di Chimica, Università di Firenze, 50144 Firenze, Italy, and Department of Chemistry and Molecular Structure Center, Indiana University, Bloomington, Indiana 47405. Received September 18, 1992

Abstract: The syntheses and electrochemical and magnetochemical properties of $[\text{Mn}_{12}\text{O}_{12}(\text{O}_2\text{CPh})_{16}(\text{H}_2\text{O})_4]$ (**3**), its solvate $3\text{-PhCOOH} \cdot \text{CH}_2\text{Cl}_2$, and $[\text{Mn}_{12}\text{O}_{12}(\text{O}_2\text{CMe})_{16}(\text{H}_2\text{O})_4] \cdot \text{MeCOOH} \cdot 3\text{H}_2\text{O}$ (**4**) are reported. Complex **3** can be prepared either by reaction of $\text{Mn}(\text{OAc})_2 \cdot 4\text{H}_2\text{O}$, benzoic acid, and NBu_4MnO_4 in pyridine or by reaction of PhCOOH with complex **4** slurried in CH_2Cl_2 . Complex **3** crystallizes in the triclinic space group $P\bar{1}$, which at -146°C has $a = 27.072(19)$ Å, $b = 17.046(11)$ Å, $c = 14.254(8)$ Å, $\alpha = 98.39(3)^\circ$, $\beta = 98.44(4)^\circ$, $\gamma = 89.27(4)^\circ$, and $Z = 2$. The structure was refined with 4814 observed [$F > 3.0\sigma(F)$] reflections to give $R = 9.54$ and $R_w = 10.07$. $[\text{Mn}_{12}\text{O}_{12}(\text{O}_2\text{CPh})_{16}(\text{H}_2\text{O})_4]$ (**3**) consists of a central $[\text{Mn}^{\text{IV}}_4\text{O}_4]^{8+}$ cubane held within a nonplanar ring of eight Mn^{III} atoms by eight $\mu_3\text{-O}^{2-}$ ions. Peripheral ligation is provided by 16 $\mu_2\text{-O}_2\text{CPh}^-$ and four terminal H_2O groups, where the four H_2O ligands are located on two Mn atoms. Four redox waves are seen in the cyclic voltammogram of complex **3** in CH_2Cl_2 : two reversible waves [an oxidation wave at 0.79 V (vs ferrocene/ferrocenium) and a reduction wave at 0.11 V] and two irreversible waves at -0.23 and -0.77 V. Complex **4** exhibits the same four redox couples in MeCN. Variable-temperature DC magnetic susceptibility data measured at 10.0 kG are presented for polycrystalline samples of complex **3** and the solvate $3\text{-PhCOOH} \cdot \text{CH}_2\text{Cl}_2$. At 320 K, μ_{eff} /molecule is $\sim 12 \mu_B$ and increases to a maximum of $\sim 20\text{--}21 \mu_B$ at ~ 10 K, whereupon μ_{eff} /molecule decreases rapidly at low temperatures. It is concluded that these complexes exhibit appreciable magnetic anisotropy. Even at fields as low as 1 kG the polycrystallites have to be restrained from torquing by embedding the polycrystalline sample in parafilm. Complexes **3** and $3\text{-PhCOOH} \cdot \text{CH}_2\text{Cl}_2$ exhibit somewhat different μ_{eff} /molecule versus temperature curves. Magnetization measurements at 20.0, 30.0, 40.0, and 50.0 kG in the 2–4 K range are used to determine that in these fields complexes **3** and $3\text{-PhCOOH} \cdot \text{CH}_2\text{Cl}_2$ have $S = 10$ and $S = 9$ ground states, respectively. A relatively large zero-field splitting is in evidence, and this was confirmed by high-field EPR experiments with a CO_2 far-infrared laser. AC susceptibility data in zero applied field are given for complexes **3** and **4** in the 4–25 K range. It is concluded that complex **3** has a $S = 9$ ground state at zero field, whereas complex **4** has a $S = 10$ ground state at zero field. The most interesting observation for complexes **3** and **4** derives from the out-of-phase (imaginary) component of the AC susceptibility, χ_M'' . Both of these complexes exhibit a nonzero χ_M'' , which when measured at various frequencies shows a maximum at different temperatures. These two complexes are the only molecular solids known to exhibit a nonzero χ_M'' in the paramagnetic phase. The results of theoretical calculations of the ordering of spin states in a $\text{Mn}_4^{\text{IV}}\text{Mn}_8^{\text{III}}$ complex, assuming reasonable values for the exchange parameters characterizing the different pairwise interactions, are presented to rationalize the $S = 8\text{--}10$ ground states.

Introduction

Considerable effort has been directed at understanding magnetic exchange interactions occurring in polynuclear transition-metal complexes.⁴ The nature (antiferromagnetic or ferromagnetic) and magnitude of a magnetic exchange interaction between two metal ions are reasonably well understood in terms of the energetics and overlap of "magnetic orbitals".^{4a} The success in understanding magnetic exchange interactions in polynuclear complexes has prompted efforts in the last few years to see if these complexes can be used as molecular building blocks for materials exhibiting interesting properties. In general, the concept of molecular-based materials is being pursued in many directions. Instead of using solids consisting of extended lattices such as in oxides, the goal

is to make up a solid lattice of molecular building blocks. With certain building blocks arranged properly in a solid lattice, it may be possible to prepare a material that exhibits interesting properties. Examples of this molecular-based materials approach can be found in the active research on organic materials with nonlinear optical properties⁵ and the studies on organic conductors and superconductors.⁶

Miller, Epstein, and co-workers⁷ have prepared organometallic ferromagnets where metallocene cations (D^+) and organic anions (A^-), each with a single unpaired electron ($S = 1/2$), are assembled in alternating stacks. The pairwise ($\text{D}^+ \cdots \text{A}^-$) magnetic exchange interactions in each stack are important, but it is the exchange

(1) Università di Firenze.
 (2) University of California at San Diego.
 (3) (a) Department of Chemistry, Indiana University. (b) Molecular Structure Center, Indiana University.
 (4) (a) *Magneto-Structural Correlation in Exchange-Coupled Systems*; Willett, R. D., Gatteschi, D., Kahn, O., Eds.; NATO ASI Series C, 140; D. Reidel Publishing Co.: Dordrecht, The Netherlands, 1985. (b) *Magnetic Molecular Materials*; Gatteschi, D., Kahn, O., Miller, J. S., Palacio, F., Eds.; NATO ASI Series E, 198; Kluwer Academic Publishers: Dordrecht, The Netherlands, 1991.

(5) (a) *Nonlinear Optical Properties of Organic Molecules and Crystals*; Chela, D. S., Zyss, J., Eds.; Academic Press: Orlando, 1987; Vols. 1 and 2. (b) Williams, J. M. *Angew. Chem., Int. Ed. Engl.* **1984**, *23*, 690. (c) *Materials for Nonlinear Optics, Chemical Perspectives*; Marder, S. R., Sohn, J. E., Stucky, G. D., Eds.; ACS Symposium Series 455; American Chemical Society: Washington, DC, 1991.

(6) (a) Bredas, J. L.; Street, G. B. *Acc. Chem. Res.* **1985**, *18*, 309. (b) Wudl, F. *Acc. Chem. Res.* **1984**, *17*, 227. (c) Torrance, J. B. *Acc. Chem. Res.* **1979**, *12*, 79. (d) Williams, J. M. *Prog. Inorg. Chem.* **1985**, *33*, 183.

(7) (a) Miller, J. S.; Epstein, A. J.; Reiff, W. M. *Chem. Rev.* **1988**, *88*, 201 and references therein. (b) Miller, J. S.; Epstein, A. J.; Reiff, W. M. *Acc. Chem. Res.* **1988**, *21*, 114 and references therein.

interactions between stacks which dictate the overall ferromagnetic ordering at low temperatures. Thus, the interstack alignment (registry) is important. When D^+ is the decamethylferrocenium cation $[Fe(C_5Me_5)_2]^+$ and A^- is the anion of tetracyanoethylene (TCNE⁻), the compound ferromagnetically orders at $T_c = 4.8$ K. Broderick et al.⁸ very recently reported that $[Mn(C_5Me_5)_2](TCNQ)$ ferromagnetically orders at $T_c = 6.2$ K.

As a second strategy for building molecular-based ferromagnetic materials, Kahn and co-workers⁹ have prepared ferromagnetic chains consisting of Cu^{II} -bridge- Mn^{II} building blocks. Again the crucial point is to arrange these chains in the solid state so that there is a net ferromagnetic coupling between chains. The two compounds $[Mn^{II}Cu^{II}(pba)(H_2O)_3] \cdot 2H_2O$ (**1**) and $[Mn^{II}Cu^{II}(pbaOH)(H_2O)_3]$ (**2**), where pba is 1,3-propylenebis(oxamato) and pbaOH is 2-hydroxy-1,3-propylenebis(oxamato), have similar chain structures. In the 30–300 K range, both **1** and **2** show magnetic susceptibilities (χ) characteristic of ferrimagnetic chains ($S = 1/2$ for Cu^{II} and $S = 5/2$ for Mn^{II}). However, for compound **1** there is a maximum of χT at 2.3 K, that is, compound **1** experiences a 3D antiferromagnetic ordering. On the other hand, compound **2** experiences a 3D ferromagnetic transition at $T_c = 4.6$ K. Below this temperature, **2** exhibits a spontaneous magnetization and a hysteresis loop characteristic of a soft magnet. The main structural difference between **1** and **2** is found in different registries between the chains.

The third successful strategy to obtain a molecular-based ferromagnet has been taken by Caneschi et al.¹⁰ Chains made of metal complexes with $S = 1/2$ nitroxide ligands have been prepared. The compound $[Mn^{II}(hfa)_2(NiTiPr)]$ ferromagnetically orders at $T_c = 7.6$ K.

The preparation of molecules with large numbers of unpaired electrons is also being pursued in many laboratories as a means of obtaining building blocks for molecular-based magnetic materials. Following Mataga's early suggestion,¹¹ Iwamura et al.¹² and Itoh et al.¹³ have prepared interesting conjugated π organic molecules that have several unpaired electrons. A hydrocarbon consisting of five carbene linkages and $S = 6$ has the highest spin multiplicity for an organic molecule.¹⁴ Dougherty and co-workers¹⁵ are preparing high-spin organic structures that have more localized bonding than that found in the conjugated π radicals. It is interesting to note that Caneschi et al.¹⁶ reported that the $[Mn_6^{II}(\text{nitroxide})_6]$ complex has a $S = 12$ ground state. Also, $[Mn_{12}O_{12}(O_2CPh)_{16}(H_2O)_4]$ (**3**) has been reported¹⁷ to have a $S = 14$ ground state in a 10-kG field. This last conclusion is shown in this paper to be incorrect due to partial torquing of polycrystallites in an external magnetic field. A smaller $S = 10$ value is found for the ground state of this Mn_{12} complex.

Very recently, Caneschi et al.¹⁸ reported that the analogous complex $[Mn_{12}O_{12}(O_2CMe)_{16}(H_2O)_4] \cdot 2(MeCO_2H) \cdot 4H_2O$ (**4**) has a $S = 10$ ground state in zero magnetic field. Schake et al.¹⁹ also communicated that it is possible to replace four of the Mn^{III} ions

in complex **4** by four Fe^{III} ions, and the resulting $Mn^{IV}_4Mn^{III}_4Fe^{III}_4$ complex has a ground state with $S \approx 2$. In the present paper, detailed magnetic susceptibility and EPR data are presented for complexes **3** and **4**. The electronic structure of these complexes is probed by means of variable-field (10 G–50 kG) SQUID susceptibility data as well as variable-frequency AC susceptibility data measured at zero field. Additional insight is gained from EPR data obtained with a far-infrared laser and approximate theoretical calculations.

Experimental Section

Compound Preparation. All chemicals and solvents were used as received; all preparations and manipulations were performed under aerobic conditions. $(NBu^*_4)[MnO_4]$ was prepared as described elsewhere.²⁰ **WARNING:** Extreme caution should be taken in the use of organic permanganates; detonation of materials during drying at elevated temperatures has been reported with some salts of MnO_4^- . Readers are referred to the Experimental Section of ref 20 for more details. $[Mn_3O(O_2CMe)_6(py)_3](ClO_4)$ (**5**) was prepared as described elsewhere.²¹

$[Mn_{12}O_{12}(O_2CPh)_{16}(H_2O)_4]$ (**3**), **Method A.** $Mn(OAc)_2 \cdot 4H_2O$ (2.00 g, 8.15 mmol) and benzoic acid (7.50 g, 61 mmol) were dissolved in pyridine (20 mL), and solid $NBu^*_4MnO_4$ (1.14 g, 3.15 mmol) added in small portions with stirring to give a dark brown solution. After a further 15 min, the solvent was removed in vacuo to give a brown oil. This was extracted with EtOH (100 mL) to give a reddish-brown solution and some undissolved brown solid that was separated by filtration. The solid brown residue was extracted into a minimum of MeCN and filtered, and the filtrate was allowed to concentrate by slow evaporation to give dark brown crystals of $[Mn_{12}O_{12}(O_2CPh)_{16}(H_2O)_4]$ (**3**) in 5–10% yield. These were collected by filtration and recrystallized from CH_2Cl_2 /hexanes to give well-formed black prisms suitable for structural studies. Crystals obtained from this procedure contain no interstitial solvate molecules. Selected IR data: 3300 (m), 1595 (s), 1560 (s), 1515 (s), 715 (s), 675 (s), 650 (s), 610 (s), 550 (m), 520 (m). Electronic spectrum in CH_2Cl_2 : λ_{max} nm (ϵ_M/Mn , $L \text{ mol}^{-1} \text{ cm}^{-1}$): 492 (610), 594 (sh, 250), 712 (100). Anal. Calcd for $C_{112}H_{88}O_{48}Mn_{12}$: C, 47.0; H, 3.1; Mn, 23.0. Found: C, 47.7; H, 3.5; Mn, 22.3.

$[Mn_{12}O_{12}(O_2CPh)_{16}(H_2O)_4]$ (**3**), **Method B.** To a slurry of $[Mn_{12}O_{12}(O_2CMe)_{16}(H_2O)_4] \cdot MeCOOH \cdot 3H_2O$ (0.50 g, 0.25 mmol) in CH_2Cl_2 (50 mL) was added $PhCOOH$ (1.0 g, 8.0 mmol). The mixture was stirred for 4 h and filtered to remove a small amount of undissolved solid. Hexanes (100 mL) were added to the filtrate, and the solution was stored overnight at room temperature; the resulting black microcrystals were collected by filtration, washed with hexanes and Et_2O , and dried in air. Anal. Calcd for $[Mn_{12}O_{12}(O_2CMe)_3(O_2CPh)_{13}(H_2O)_4] \cdot MeCOOH$: C, 43.48; H, 3.17; Mn, 24.10. Found: C, 43.70; H, 2.90; Mn, 24.20. The above treatment with excess $PhCOOH$ was then repeated employing the black microcrystals and the same reaction solvent and reagent ratios. The resulting black microcrystals of $[Mn_{12}O_{12}(O_2CPh)_{16}(H_2O)_4] \cdot PhCOOH \cdot CH_2Cl_2$ were collected by filtration, washed with hexanes and diethyl ether, and dried in vacuo. The overall yield was ~52%. Anal. Calcd for $C_{120}H_{90}O_{50}Cl_2Mn_{12}$: C, 46.98; H, 3.15; Mn, 21.49. Found: C, 46.8; H, 3.2; Mn, 21.2.

$[Mn_{12}O_{12}(O_2CMe)_{16}(H_2O)_4] \cdot MeCO_2H \cdot 4H_2O$ (**4**). This complex was prepared by the published procedure.²² The same product is also obtainable by a related procedure. A solution of $[Mn_3O(O_2CMe)_6(py)_3](ClO_4)$ (1.00 g, 1.15 mmol) in 60% $MeCOOH/H_2O$ (v/v) was treated with solid $KMnO_4$ (0.046 g, 0.29 mmol) in small portions to give an essentially black solution. The latter was heated slowly to 60 °C and then allowed to cool slowly to ambient temperature and left undisturbed for 2 h. The resulting black needles were collected by filtration, washed copiously with acetone and THF, and dried in air. The yield was ~80%. (The copious washing has been found essential to remove excess acetic acid and prevent slow decomposition on storage to a sticky, insoluble brown solid). An analytical sample dried in vacuum was analyzed for the formulation $[Mn_{12}O_{12}(O_2CMe)_{16}(H_2O)_4] \cdot MeCOOH \cdot 3H_2O$, suggesting partial loss of solvent molecules of crystallization, and this formula weight was therefore employed for reactions with benzoic acid. Anal. Calcd for $C_{34}H_{66}O_{33}Mn_{12}$: C, 20.60; H, 3.36; Mn, 33.26. Found: C, 20.99; H, 3.53; Mn, 33.22.

X-ray Crystallography and Structure Solution for Complex 3. Data on complex **3** were collected on a Picker four-circle diffractometer at approximately -146 °C; details of the diffractometry, low-temperature

(8) Broderick, W. E.; Thompson, J. A.; Day, E. P.; Hoffman, B. M. *Science* **1990**, *249*, 401.

(9) (a) Kahn, O. *Struct. Bonding (Berlin)* **1987**, *68*, 89 and references therein. (b) Kahn, O.; Pei, Y.; Nakatani, K.; Journaux, Y. *Mol. Cryst. Liq. Cryst.* **1989**, *176*, 481.

(10) Caneschi, A.; Gatteschi, D.; Sessoli, R. *Acc. Chem. Res.* **1989**, *22*, 392 and references therein.

(11) Mataga, N. *Theor. Chim. Acta* **1968**, *10*, 372.

(12) (a) Iwamura, H. *Pure Appl. Chem.* **1987**, *59*, 1595 and references therein. (b) Iwamura, H. *Pure Appl. Chem.* **1986**, *58*, 187 and references therein.

(13) Itoh, K.; Takui, T.; Teki, Y.; Kinoshita, J. *J. Mol. Elect.* **1988**, *4*, 181.

(14) Nakamura, N.; Inoue, K.; Iwamura, H.; Fujioka, T.; et al. *J. Am. Chem. Soc.* **1992**, *114*, 1484.

(15) Dougherty, D. A. *Pure Appl. Chem.* **1990**, *62*, 519.

(16) Caneschi, A.; Gatteschi, D.; Laugier, J.; Rey, P.; Sessoli, R.; Zanchini, C. *J. Am. Chem. Soc.* **1988**, *110*, 2795.

(17) Boyd, P. D. W.; Li, Q.; Vincent, J. B.; Folting, K.; Chang, H.-R.; Streib, W. E.; Huffman, J. C.; Christou, G.; Hendrickson, D. N. *J. Am. Chem. Soc.* **1988**, *110*, 8537.

(18) Caneschi, A.; Gatteschi, D.; Sessoli, R.; Barra, A. L.; Brunel, L. C.; Guillot, M. *J. Am. Chem. Soc.* **1991**, *113*, 5873.

(19) Schake, A. R.; Tsai, H.-L.; De Vries, N.; Webb, R. J.; Folting, K.; Hendrickson, D. N.; Christou, G. *J. Chem. Soc., Chem. Commun.* **1992**, 181.

(20) Sala, T.; Sargent, M. V. *J. Chem. Soc., Chem. Commun.* **1978**, 253.

(21) Vincent, J. B.; Chang, H.-R.; Folting, K.; Huffman, J. C.; Christou, G.; Hendrickson, D. N. *J. Am. Chem. Soc.* **1987**, *109*, 5703 and references therein.

(22) Lis, T. *Acta Crystallogr. Sect. B* **1980**, *36*, 2042.

Table I. Crystallographic Data for $[\text{Mn}_{12}\text{O}_{12}(\text{O}_2\text{CPh})_{16}(\text{H}_2\text{O})_4]$ (3)

parameter	value
formula	$\text{C}_{112}\text{H}_{88}\text{O}_{48}\text{Mn}_{12}$
molar mass, $\text{g}\cdot\text{mol}^{-1}$	2861.22
crystal system	triclinic
space group	$P\bar{1}$
t , °C	-146
a , Å	27.072(19) ^a
b , Å	17.046(11)
c , Å	14.254(8)
α , deg	98.39(3)
β , deg	98.44(4)
γ , deg	89.27(4)
Z	2
V , Å ³	6436.7
crystal size, mm	0.40 × 0.20 × 0.20
radiation (Mo K α), Å	0.710 69 ^b
abs coeff, cm^{-1}	11.68
scan speed, deg min^{-1}	6.0
scan width, deg	1.5 plus dispersion
total data	23 283
unique data	16 901
averaging R^c	0.09
obsd data, $F > 3.0\sigma(F)$	4814
R (R_w), %	9.54 (10.07) ^d
goodness of fit	1.472

^a 36 reflections at -146 °C. ^b Graphite monochromator. ^c Reflections measured more than once. ^d No absorption correction performed.

facilities, and computational procedures employed by the Molecular Structure Center are available elsewhere.²³ Data collection parameters are summarized in Table I. A systematic search of a limited hemisphere of reciprocal space yielded a set of reflections which exhibited no symmetry or systematic absences. The choice of the centrosymmetric triclinic space group $P\bar{1}$ was confirmed by the subsequent solution and refinement of the structure. A total of 23 283 reflections were collected. Following Lorentz-polarization correction and averaging of equivalent reflections, 16 901 unique reflections remained. Due to the relatively poor quality of the crystal, only 4814 reflections had $F > 3.0\sigma(F)$, and these were used in the subsequent solution and refinement of the structure.

The structure was solved by direct methods (MULTAN) and Fourier techniques. All nonhydrogen atoms were readily located. Due to the large number of independent atoms (172), the low quantity of data, and computer program space limitations, no attempt to locate or include hydrogen atoms was made and no atoms were refined with anisotropic thermal parameters; the structure was thus refined using full-matrix least squares with isotropic thermal parameters on all atoms. Final values of conventional discrepancy indices R and R_w are included in Table I. The final difference map was essentially featureless except for several peaks of approximately $1 \text{ e}/\text{Å}^3$ near the Mn atoms.

Physical Measurements. DC magnetic susceptibility measurements were carried out on a Quantum Design MPMS SQUID susceptometer equipped with a 5.5 T magnet and operating in the range of 1.6–400 K. The home-built AC susceptometer operates in the range of 4–25 K in zero applied field. The frequency dependence of the imaginary component of the AC susceptibility was also determined in the range of 55–500 Hz. EPR spectra were recorded at frequencies of 8.2, 9.8, 11.7, 14.3, and 17.5 cm^{-1} with a far-infrared CO_2 laser spectrometer.²⁴

Pascal's constants²⁵ were used to estimate the diamagnetic corrections for each complex, which were subtracted from the experimental susceptibilities to give the molar paramagnetic susceptibilities. The computer program GENSPIN²⁶ was used to analyze variable-field magnetization data. The spin of the ground state is set at some value, and then the spin Hamiltonian matrix is diagonalized at each magnetic field to fit the experimental data. The computer program CLUMAG²⁷ was used to calculate the energies of spin states for a $\text{Mn}_4^{\text{IV}}\text{Mn}_8^{\text{III}}$ complex.

Electrochemical studies were performed by using an IBM Model EC 225 voltammetric analyzer, a PAR Model 175 Universal Programmer,

Table II. Selected^a Interatomic Distances for $[\text{Mn}_{12}\text{O}_{12}(\text{O}_2\text{CPh})_{16}(\text{H}_2\text{O})_4]$ (3)

A	B	distance (Å)	A	B	distance (Å)
Mn(1)	Mn(2)	2.820(7)	Mn(6)	O(19)	1.929(20)
Mn(1)	Mn(3)	2.981(7)	Mn(7)	O(19)	1.880(21)
Mn(1)	Mn(4)	2.834(7)	Mn(7)	O(20)	1.896(20)
Mn(1)	Mn(5)	2.809(7)	Mn(8)	O(20)	1.866(21)
Mn(1)	Mn(6)	3.441(2)	Mn(8)	O(21)	1.872(21)
Mn(1)	Mn(12)	3.442(7)	Mn(8)	O(25)	2.238(20)
Mn(2)	Mn(3)	2.821(7)	Mn(8)	O(26)	2.183(21)
Mn(2)	Mn(4)	3.000(7)	Mn(9)	O(21)	1.922(21)
Mn(2)	Mn(6)	3.487(7)	Mn(9)	O(22)	1.874(21)
Mn(2)	Mn(7)	2.775(7)	Mn(10)	O(22)	1.847(20)
Mn(2)	Mn(8)	3.479(7)	Mn(10)	O(23)	1.875(21)
Mn(3)	Mn(4)	2.817(7)	Mn(11)	O(23)	1.921(21)
Mn(3)	Mn(8)	3.439(7)	Mn(11)	O(24)	1.906(21)
Mn(3)	Mn(9)	2.803(7)	Mn(12)	O(17)	1.878(21)
Mn(3)	Mn(10)	3.454(7)	Mn(10)	Mn(11)	3.312(7)
Mn(4)	Mn(10)	3.456(7)	Mn(11)	Mn(12)	3.398(7)
Mn(4)	Mn(11)	2.813(7)	Mn(1)	O(13)	1.899(21)
Mn(4)	Mn(12)	3.460(7)	Mn(1)	O(14)	1.925(20)
Mn(5)	Mn(6)	3.315(7)	Mn(1)	O(16)	1.966(19)
Mn(5)	Mn(12)	3.382(7)	Mn(1)	O(17)	1.839(22)
Mn(6)	Mn(7)	3.327(7)	Mn(1)	O(18)	1.857(20)
Mn(7)	Mn(8)	3.386(7)	Mn(2)	O(13)	1.915(21)
Mn(8)	Mn(9)	3.406(7)	Mn(2)	O(14)	1.924(20)
Mn(9)	Mn(10)	3.285(7)	Mn(2)	O(15)	1.938(19)
Mn(3)	O(22)	1.883(20)	Mn(2)	O(19)	1.838(20)
Mn(4)	O(14)	1.955(19)	Mn(2)	O(20)	1.907(21)
Mn(4)	O(15)	1.908(20)	Mn(3)	O(13)	1.988(2)
Mn(4)	O(16)	1.906(20)	Mn(3)	O(15)	1.880(20)
Mn(4)	O(23)	1.847(20)	Mn(3)	O(16)	1.888(20)
Mn(4)	O(24)	1.849(22)	Mn(3)	O(21)	1.851(21)
Mn(5)	O(17)	1.921(21)	Mn(12)	O(24)	1.910(21)
Mn(5)	O(18)	1.898(21)	Mn(12)	O(27)	2.201(22)
Mn(5)	O(30)	2.200(20)	Mn(12)	O(28)	2.232(22)
Mn(6)	O(18)	1.896(20)			

^a For the $\text{Mn}_{12}\text{O}_{12}$ core and H_2O molecules only; a full listing is available in the supplementary material.

and a standard three-electrode assembly (glassy-carbon working, Pt-wire auxiliary, SCE reference) with 0.1 M NBu_4PF_6 as supporting electrolyte. No IR compensation was employed. Quoted potential values are vs the ferrocene/ferrocenium couple under the same conditions. The scan rate was set at 100 mV/s. The solvent used was distilled CH_2Cl_2 for $[\text{Mn}_{12}\text{O}_{12}(\text{O}_2\text{CPh})_{16}(\text{H}_2\text{O})_4]$ and MeCN for $[\text{Mn}_{12}\text{O}_{12}(\text{OAc})_{16}(\text{H}_2\text{O})_4]$. The concentration of the complexes was 1 mM.

Results

Two procedures have been developed for the preparation of $[\text{Mn}_{12}\text{O}_{12}(\text{O}_2\text{CPh})_{16}(\text{H}_2\text{O})_4]$ (3). The first is a low yield (5–10%) direct synthesis from $\text{Mn}(\text{O}_2\text{CMe})_2\cdot 4\text{H}_2\text{O}$, $\text{NBu}_4^+\text{MnO}_4^-$, and PhCOOH in pyridine. An alternative and superior procedure is ligand substitution of MeCOO^- with PhCOO^- on treatment of $[\text{Mn}_{12}\text{O}_{12}(\text{O}_2\text{CMe})_{16}(\text{H}_2\text{O})_4]\cdot 2\text{MeCOOH}\cdot 4\text{H}_2\text{O}$ (4) with excess PhCOOH . The single-crystal X-ray structure of 3 has been determined at -146 °C. Crystallographic data and selected structural parameters are given in Tables I–IV; a labeled figure and space-filling stereoviews are given in Figures 1 and 2, respectively. Electrochemical studies on 3 and 4 have been performed using cyclic voltammetry (CV) and differential pulse voltammetry (DPV). The observed scans are shown in Figures 4 and 5.

Variable-temperature DC magnetic susceptibility data were collected for several different samples of complex 3 at an applied magnetic field of 1 T (10 kG), see Figure 6. Unrestrained polycrystalline samples as well as samples of 3 embedded in paraffin wax were examined. As can be seen in Figure 6, the effective magnetic moment (μ_{eff}) per Mn_{12} complex 3 is $\sim 12 \mu_B$ at 320 K. As the temperature is decreased, the value of μ_{eff} /molecule initially decreases and then increases to a maximum in the 15–20 K range. The maximum value of μ_{eff} /molecule varies from ~ 20 to $\sim 23 \mu_B$ depending on the sample condition.

The possibility of hysteresis effects was examined by measuring the DC magnetic susceptibility from 100 to 2000 G of a paraffin-embedded sample of complex 3 maintained at 5.00 K, see

(23) Chisholm, M. F.; Folting, K.; Huffman, J. C.; Kirkpatrick, C. C. *Inorg. Chem.* **1984**, *23*, 1021.

(24) (a) Muller, F.; Hopkins, M. A.; Coron, N.; Grynberg, M.; Brunel, L. C.; Matrinez *Rev. Sci. Instrum.* **1989**, *60*, 3681. (b) Barra, A. L.; Brunel, L. C.; Robert, J. B. *Chem. Phys. Lett.* **1990**, *165*, 107.

(25) *Theory and Applications of Molecular Paramagnetism*, Boudreaux, E. A., Mulay, L. N., Eds.; J. Wiley & Sons: New York, 1976.

(26) Schmitt, E. A.; Hendrickson, D. N., unpublished results.

(27) Gatteschi, D.; Pardi, L. *Gazz. Chim. Ital.* In press.

Table III. Selected^a Angles for $[Mn_{12}O_{12}(O_2CPh)_{16}(H_2O)_4]$ (3)

A	B	C	angle (deg)	A	B	C	angle (deg)	A	B	C	angle (deg)
O(13)	Mn(1)	O(14)	84.6(9)	O(17)	Mn(12)	O(24)	91.3(9)	O(15)	Mn(4)	O(16)	82.3(9)
O(13)	Mn(1)	O(16)	79.4(8)	Mn(1)	O(13)	Mn(2)	95.3(10)	O(15)	Mn(4)	O(23)	96.2(9)
O(13)	Mn(1)	O(17)	173.8(10)	Mn(1)	O(13)	Mn(3)	100.1(9)	O(15)	Mn(4)	O(24)	170.5(9)
O(13)	Mn(1)	O(18)	97.9(9)	Mn(2)	O(13)	Mn(3)	92.6(9)	O(16)	Mn(4)	O(23)	90.7(9)
O(14)	Mn(1)	O(16)	84.3(8)	Mn(1)	O(14)	Mn(2)	94.2(9)	O(16)	Mn(4)	O(24)	88.2(9)
O(14)	Mn(1)	O(17)	89.6(9)	Mn(1)	O(14)	Mn(4)	93.9(8)	O(23)	Mn(4)	O(24)	84.1(9)
O(14)	Mn(1)	O(18)	92.1(9)	Mn(2)	O(14)	Mn(4)	101.3(9)	O(17)	Mn(5)	O(18)	81.3(9)
O(16)	Mn(1)	O(17)	97.7(9)	Mn(2)	O(15)	Mn(3)	95.3(9)	O(18)	Mn(6)	O(19)	92.4(9)
O(16)	Mn(1)	O(18)	175.7(9)	Mn(2)	O(15)	Mn(4)	102.5(9)	O(19)	Mn(7)	O(20)	83.7(9)
O(17)	Mn(1)	O(18)	84.6(9)	Mn(3)	O(15)	Mn(4)	96.1(9)	Mn(5)	O(18)	Mn(6)	121.8(11)
O(13)	Mn(2)	O(14)	84.2(9)	Mn(1)	O(16)	Mn(3)	101.3(9)	Mn(2)	O(19)	Mn(6)	135.6(12)
O(13)	Mn(2)	O(15)	84.9(9)	Mn(1)	O(16)	Mn(4)	94.1(9)	Mn(2)	O(19)	Mn(7)	96.6(10)
O(13)	Mn(2)	O(19)	89.5(9)	Mn(3)	O(16)	Mn(4)	95.9(9)	Mn(6)	O(19)	Mn(7)	121.8(11)
O(13)	Mn(2)	O(20)	87.0(9)	Mn(1)	O(17)	Mn(5)	96.6(10)	Mn(2)	O(20)	Mn(7)	93.7(9)
O(14)	Mn(2)	O(15)	78.1(8)	Mn(1)	O(17)	Mn(12)	135.7(12)	Mn(2)	O(20)	Mn(8)	134.5(11)
O(14)	Mn(2)	O(19)	96.1(9)	Mn(5)	O(17)	Mn(12)	125.8(12)	Mn(7)	O(20)	Mn(8)	128.3(12)
O(14)	Mn(2)	O(20)	171.1(9)	Mn(1)	O(18)	Mn(5)	96.9(10)	Mn(3)	O(21)	Mn(8)	135.0(12)
O(15)	Mn(2)	O(19)	172.3(9)	Mn(1)	O(18)	Mn(6)	133.0(1)	Mn(3)	O(21)	Mn(9)	95.9(10)
O(15)	Mn(2)	O(20)	100.4(8)	O(15)	Mn(3)	O(16)	83.6(9)	Mn(8)	O(21)	Mn(9)	127.7(11)
O(19)	Mn(2)	O(20)	84.5(9)	O(15)	Mn(3)	O(21)	89.8(9)	Mn(3)	O(22)	Mn(9)	96.5(9)
O(13)	Mn(3)	O(15)	84.5(9)	O(15)	Mn(3)	O(22)	91.3(9)	Mn(3)	O(22)	Mn(10)	133.7(12)
O(13)	Mn(3)	O(16)	79.1(8)	O(16)	Mn(3)	O(21)	173.1(9)	Mn(9)	O(22)	Mn(10)	122.4(11)
O(13)	Mn(3)	O(21)	98.4(9)	O(16)	Mn(3)	O(22)	97.9(9)	Mn(4)	O(23)	Mn(10)	136.4(12)
O(13)	Mn(3)	O(22)	175.0(9)	O(21)	Mn(3)	O(22)	84.2(9)	Mn(4)	O(23)	Mn(11)	96.6(10)
O(20)	Mn(8)	O(21)	91.4(9)	O(14)	Mn(4)	O(15)	78.1(8)	Mn(10)	O(23)	Mn(11)	121.5(11)
O(21)	Mn(9)	O(22)	82.5(9)	O(14)	Mn(4)	O(16)	85.1(8)	Mn(4)	O(24)	Mn(11)	97.0(10)
O(22)	Mn(10)	O(23)	92.5(9)	O(14)	Mn(4)	O(23)	173.3(9)	Mn(4)	O(24)	Mn(12)	134.0(12)
O(23)	Mn(11)	O(24)	80.6(9)	O(14)	Mn(4)	O(24)	101.0(9)	Mn(11)	O(24)	Mn(12)	125.8(11)

^a For the $Mn_{12}O_{12}$ core only; a full listing is available in the supplementary material.

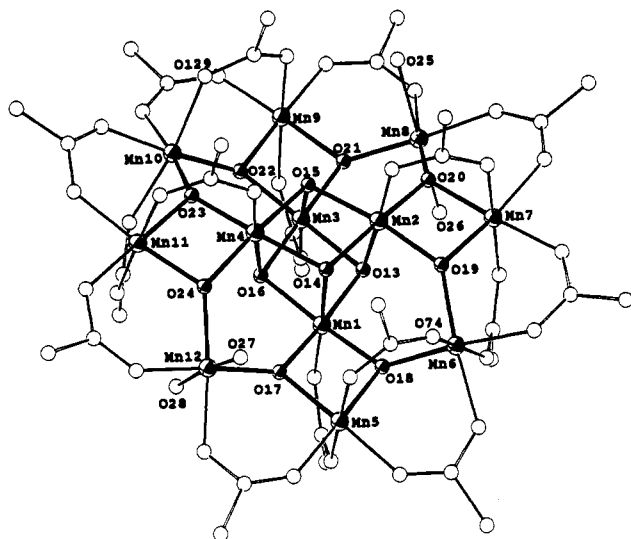


Figure 1. ORTEP representation of $[Mn_{12}O_{12}(O_2CPh)_{16}(H_2O)_4]$ (3) at the 50% probability level. For clarity, the peripheral carboxylates are deemphasized and only one phenyl carbon atoms is included. To avoid congestion, only the $[Mn_{12}O_{12}(H_2O)_4]$ core atoms are labeled plus O(74) and O(129), which are referred to in the text. A fully-labeled figure is available in the supplementary material.

Figure 7. The sample was first cooled to 5.00 K in the absence of a field. After thermal equilibration, a field of 100 G was applied and the susceptibility was measured. The external field was then increased in increments up to 2000 G. At each field it took 4 min for a measurement. After the measurement at 2000 G, the field was decreased in increments down to 100 G.

A determination of variable-field magnetization data measured at low temperatures can be useful in establishing the ground state of a polynuclear complex. Samples mixed in petroleum jelly as well as embedded in parafilm were examined. This was done to prevent small crystallites from torquing in the external magnetic field. Because a small sample of 2–3 mg was mixed in the petroleum jelly, the exact mass of the sample was determined by measuring the magnetic susceptibility of the sample at several temperatures in a field of 10.0 kG and using data measured for

Table IV. Averaged Selected Structural Parameters for $[Mn_{12}O_{12}(O_2CPh)_{16}(H_2O)_4]$ (3)

parameter	value ^a
$Mn^{IV} \cdots Mn^{IV}$ (eq)	2.991(1)
$Mn^{IV} \cdots Mn^{IV}$ (ax)	2.823(11)
$Mn^{IV} \cdots Mn^{III c}$	3.457(3)
$Mn^{IV} \cdots Mn^{III d}$	2.800(25)
$Mn^{III} \cdots Mn^{III}$	3.351(66)
$Mn^{III} - O_c$ (eq)	1.933(55)
$Mn^{IV} - O_c$ (ax)	1.907(27)
$Mn^{IV} - O_r$	1.859(76)
$Mn^{III} - O_c^c$	1.888(41)
$Mn^{III} - O_d^d$	1.902(28)
$Mn^{III} - O_w$	2.214(31)
$Mn^{IV} - O_b$	1.919(47)
$Mn^{III} - O_{b,ax}$	2.176(85)
$Mn^{III} - O_{b,eq}$	1.955(61)
$Mn^{IV} - O_c - Mn^{IV}$ (eq)	101.3(1.2)
$Mn^{IV} - O_c - Mn^{IV}$ (ax)	94.0(1.3)
$Mn^{IV} - O_r - Mn^{III c}$	134.7(1.7)
$Mn^{IV} - O_r - Mn^{III d}$	96.2(2.5)
$Mn^{III} - O_r - Mn^{III}$	124.4(3.9)
$O_c - Mn^{IV} - O_c$ (eq)	78.7(0.7)
$O_c - Mn^{IV} - O_c$ (ax)	84.2(1.9)
$O_r - Mn^{IV} - O_r$	84.4(0.3)
$O_r - Mn^{IV} - O_r^c$	91.9(0.6)
$O_r - Mn^{III} - O_r^d$	82.0(1.7)

^a Averaged using the virtual D_{2d} symmetry of the $[Mn_{12}O_{12}]$ core; numbers in parentheses are the greatest deviation of an individual value from the mean. Bond lengths in angstroms, angles in degrees. ^b O_c = central cubane oxygens; O_r = outer ring oxygens; O_w = water oxygens; O_b = benzoate oxygens; ax = axial; eq = equatorial. ^c Mn(6,8,10,12). ^d Mn(5,7,9,11).

a larger polycrystalline sample to calculate the mass. In the case of the parafilm-embedded sample, a larger sample (~10–20 mg) could be used and the mass of the sample could be measured directly. Plots of reduced magnetization ($M/N\mu_B$) versus temperature are shown in Figure 8 for two parafilm-embedded samples of complex 3, one of which is not solvated and the other is solvated with one molecule of PhCOOH.

The temperature dependence of the magnetic susceptibility of complexes 3 and 4 was measured in zero applied field with an AC susceptometer in the range of 4–25 K. Figures 9 and 10

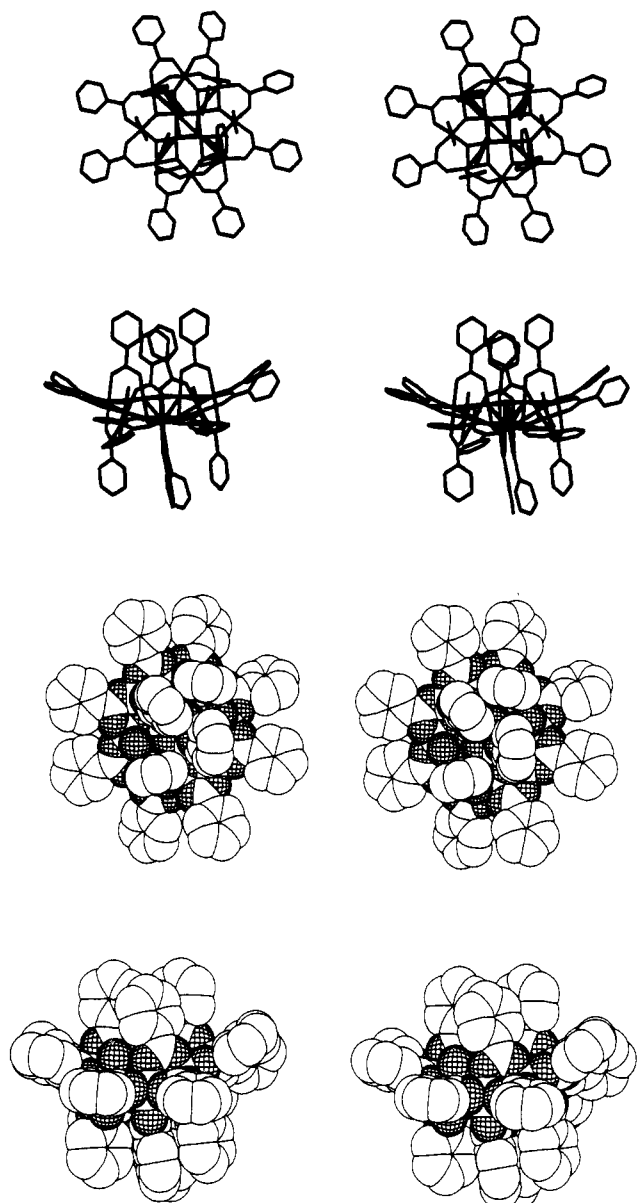


Figure 2. Stick and space-filling stereoviews of $[\text{Mn}_{12}\text{O}_{12}(\text{O}_2\text{CPh})_{16}(\text{H}_2\text{O})_4]$ (**3**) from two viewpoints, approximately axial and equatorial, emphasizing the nonplanarity of the outer ring of eight Mn^{III} atoms and the disposition of the phenyl rings.

illustrate the data for complexes **3** and **4**, respectively. The real component of the AC susceptibility is χ' . For complex **3** the value of $\chi'T$ is almost constant at $\sim 41 \text{ emu K mol}^{-1}$ ($\mu_{\text{eff}} = 17.2 \mu_{\text{B}}$), and below 6 K it decreases rapidly. The decrease is determined by the onset of relaxation effects which show up as a nonzero imaginary component of the AC susceptibility, χ'' . The temperature dependence of χ'' for complex **3** is shown in the inset of Figure 9 at 100 and 500 Hz. The value of χ'' goes through a maximum at 4.9 K for 100 Hz and 5.5 K for 500 Hz.

The zero-field magnetic susceptibility of complex **4** is higher than that of complex **3**, as shown by Figure 10. The value of $\chi'T$ increases slowly upon decreasing the temperature, reaches a plateau at $52.3 \text{ emu K mol}^{-1}$ ($\mu_{\text{eff}} = 20.4 \mu_{\text{B}}$), and then decreases below 8 K due to relaxation effects. The value of χ'' goes through a maximum which is frequency dependent: 5.4 K at 55 Hz, 6.0 K at 100 Hz, and 7.0 K at 500 Hz.

Polycrystalline powder EPR spectra of complexes **3** and **4** were recorded with a high-field spectrometer operating with a CO_2 far-infrared laser. When precautions were taken in order to avoid orientation of the crystallites, one prominent feature was observed for complexes **3** and **4**, whose resonance fields are linearly de-

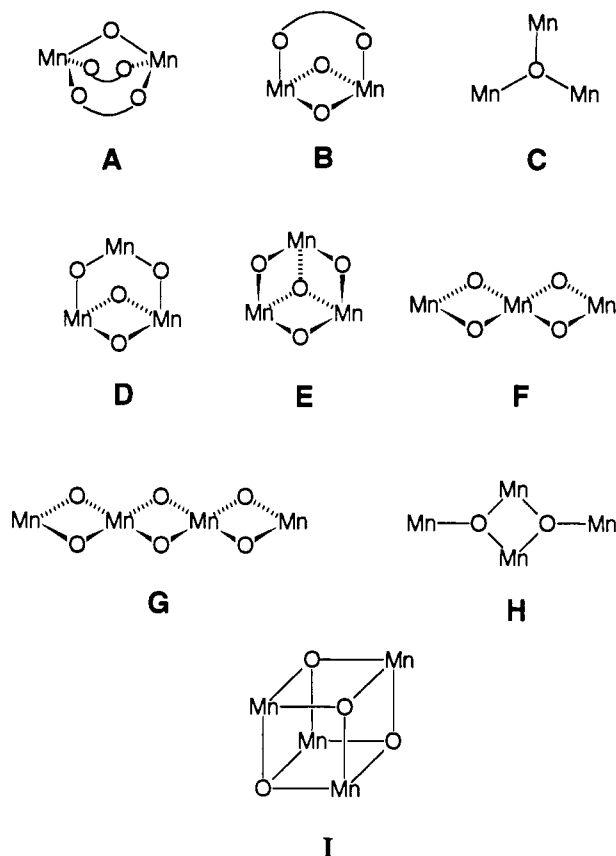


Figure 3. Nine Mn/O units that can be observed as subfragments within the $[\text{Mn}_{12}\text{O}_{12}]$ core of $[\text{Mn}_{12}\text{O}_{12}(\text{O}_2\text{CPh})_{16}(\text{H}_2\text{O})_4]$ (**3**).

pendent on frequency, as shown in Figure 11. Linear regression shows that the resonance field goes to 0 at $B_0 = 11.7 \text{ T}$ for complex **3** and at $B_0 = 10.9 \text{ T}$ for complex **4**. Other weaker features are observed for both compounds which also are linearly dependent on the frequency with the same slope. They are separated from the main feature by 1.2 T for complex **3** and by 1.4 T for complex **4**.

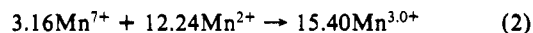
Discussion

Compound Preparation. The procedure reported by Lis in 1980 for the preparation of $[\text{Mn}_{12}\text{O}_{12}(\text{O}_2\text{CMe})_{16}(\text{H}_2\text{O})_4] \cdot 2\text{MeCOOH} \cdot 4\text{H}_2\text{O}$ (**4**) is a very convenient one that allows ready access to high yields of crystalline material.²² Although no yield was reported in the original paper, we find that this procedure, the reaction of $\text{Mn}(\text{O}_2\text{CMe})_2 \cdot 4\text{H}_2\text{O}$ with KMnO_4 in 60% acetic acid, and slight modifications thereof, allow yields of $\sim 80\%$ to be routinely obtained. Other than partial loss of molecules of crystallization on drying under vacuum, the black crystals are stable to long-term storage as long as all traces of excess acetic acid are removed by thorough washing during the isolation procedure.

The preparative method used by Lis is similar to that routinely employed for preparing manganese(III) acetate,²⁸ " $\text{Mn}(\text{O}_2\text{CMe})_3 \cdot 2\text{H}_2\text{O}$ ", except that the $\text{MnO}_4^-:\text{Mn}(\text{O}_2\text{CMe})_2$ ratio (eq 1) is increased to a value appropriate for the +3.33 average Mn



oxidation state in **4** (8 Mn^{III} , 4 Mn^{IV}). The ratio employed for " $\text{Mn}(\text{O}_2\text{CMe})_3 \cdot 2\text{H}_2\text{O}$ " is appropriate for its +3.0 oxidation state (eq 2). Since " $\text{Mn}(\text{O}_2\text{CMe})_3 \cdot 2\text{H}_2\text{O}$ " is really a polymer con-



taining $[\text{Mn}_3\text{O}(\text{O}_2\text{CMe})_6]^+$ units, it seems reasonable to suspect that the preparation of **4** proceeds by initial formation of trinuclear

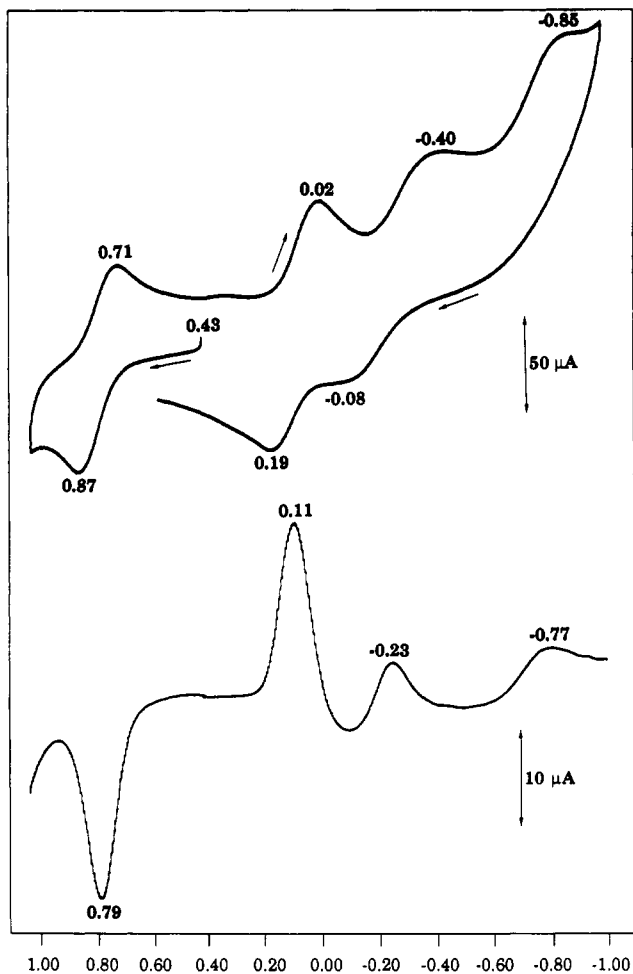
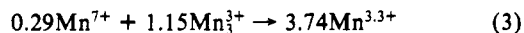


Figure 4. Cyclic voltammogram (top) and differential pulse voltammogram (bottom) of $[Mn_{12}O_{12}(O_2CPh)_{16}(H_2O)_4]$ (3) in CH_2Cl_2 . The indicated potentials are given versus the Cp_2Fe/Cp_2Fe^+ couple measured under the same conditions.

$[Mn_3O(O_2CMe)_6]^+$ -containing species and that the dodecanuclear product 4 is formed on oxidation of these by remaining MnO_4^- . Some support for this is provided in the Experimental Section, viz the oxidation of $[Mn_3O(O_2CMe)_6(py)_3](ClO_4)$ by $KMnO_4$ in a ratio designed to give 4 (eq 3). This procedure is high yield ($\sim 80\%$) but requires prior formation of the trinuclear complex and has, therefore, not been employed by us on a routine basis.



The benzoate analogue of 4, complex 3, was originally obtained¹⁷ in small yield (5–10%) from a comproportionation reaction in pyridine (Method A in the Experimental Section) between $Mn(O_2CMe)_2 \cdot 4H_2O$ and NBu_4MnO_4 in which the major product was $[Mn_3O(O_2CPh)_6(py)_3](ClO_4)$. The $MnO_4^-:Mn(O_2CMe)_2$ ratio was identical to that in eq 1, but, in this case, only a small amount of higher ($>III$) average oxidation state product was obtained. The Mn_3O product is readily removed by EtOH, leaving complex 4. Although nicely crystalline material is available by this route, it was clear that an improved preparative method was necessary to allow convenient access to greater amounts. Facile ligand substitution of bound $MeCOO^-$ with $PhCOO^-$ by treatment with excess $PhCOOH$ is a common property of $Mn/O/MeCOO^-$ complexes,^{29–31} and it suggested a means of obtaining 3 from 4. Treatment of complex 4 with 32 equiv (100% excess) of $PhCOOH$

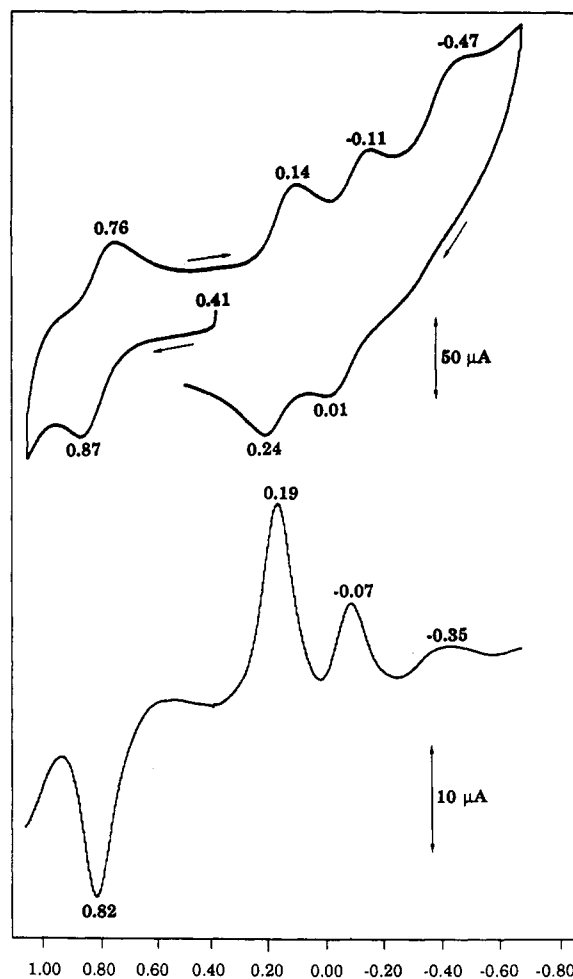
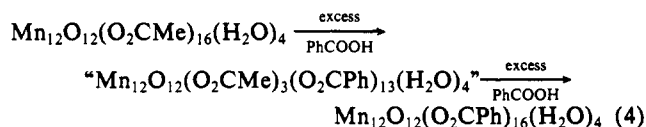


Figure 5. Cyclic voltammogram (top) and differential pulse voltammogram (bottom) of $[Mn_{12}O_{12}(O_2CMe)_{16}(H_2O)_4] \cdot 2MeCO_2H \cdot 4H_2O$ (4) in MeCN. The potentials are given versus the Cp_2Fe/Cp_2Fe^+ couple under the same conditions.

in CH_2Cl_2 leads to a majority, but not all, of the $MeCOO^-$ groups being exchanged. The black solid obtained analyzed well for “ $[Mn_{12}O_{12}(O_2CMe)_3(O_2CPh)_{13}(H_2O)_4] \cdot MeCOOH$ ”; the latter is undoubtedly the bulk analysis of a mixture of species with various levels of $MeCOO^-$ content. Another ligand substitution cycle was therefore performed; the partially exchanged solid from the first cycle was treated with 32 equiv of $PhCOOH$ ($\sim 1000\%$ excess), and the resulting product now analyzed well for the completely exchanged product $3 \cdot PhCOOH \cdot CH_2Cl_2$. The conversion is summarized in eq 4. The overall yield of the conversion



of 4 to 3 is $\sim 52\%$. Since complex 4 is available in $>80\%$ yield from a one-pot reaction, this route to 3 is overall high-yield and convenient, and it is thus the one we now routinely employ.

The interstitial $PhCOOH$ molecule obtained via the ligand substitution can be removed by recrystallization. Thus, recrystallization of $3 \cdot PhCOOH \cdot CH_2Cl_2$ from CH_2Cl_2 /hexanes gives complex 3 as in Method A, i.e., no interstitial $PhCOOH$ or CH_2Cl_2 . In contrast, recrystallization from CH_2Cl_2 /hexanes containing added $PhCOOH$ leads to recovery of $3 \cdot PhCOOH \cdot CH_2Cl_2$.

Description of Structure. Complex 3 crystallizes in the triclinic space group $P1$ and contains discrete $[Mn_{12}O_{12}(O_2CPh)_{16}(H_2O)_4]$ units with no imposed symmetry. Selected bond distances and angles are listed in Tables II and III; a more complete listing is

(29) Vincent, J. B.; Christmas, C.; Chang, H.-R.; Li, Q.; Boyd, P. D. W.; Huffman, J. C.; Hendrickson, D. N.; Christou, G. *J. Am. Chem. Soc.* **1989**, *111*, 2086.

(30) Christou, G. *Acc. Chem. Res.* **1989**, *22*, 328.

(31) Libby, E.; McCusker, J. K.; Schmitt, E. A.; Folting, K.; Hendrickson, D. N.; Christou, G. *Inorg. Chem.* **1991**, *30*, 3486.

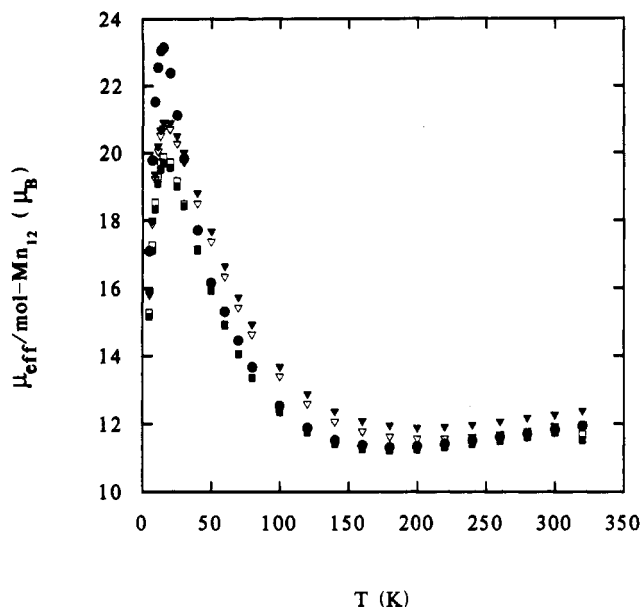


Figure 6. Plots of effective magnetic moment per Mn_{12} molecule versus temperature for five different samples of $[\text{Mn}_{12}\text{O}_{12}(\text{O}_2\text{CPh})_{16}(\text{H}_2\text{O})_4]$ (3): (●) unrestrained polycrystalline sample; (▽ and ▼) two parafilm-embedded polycrystalline samples of the nonsolvated complex; and (□ and ■) two parafilm-embedded polycrystalline samples of the solvated complex $3\text{-PhCOOH}\cdot\text{CH}_2\text{Cl}_2$.

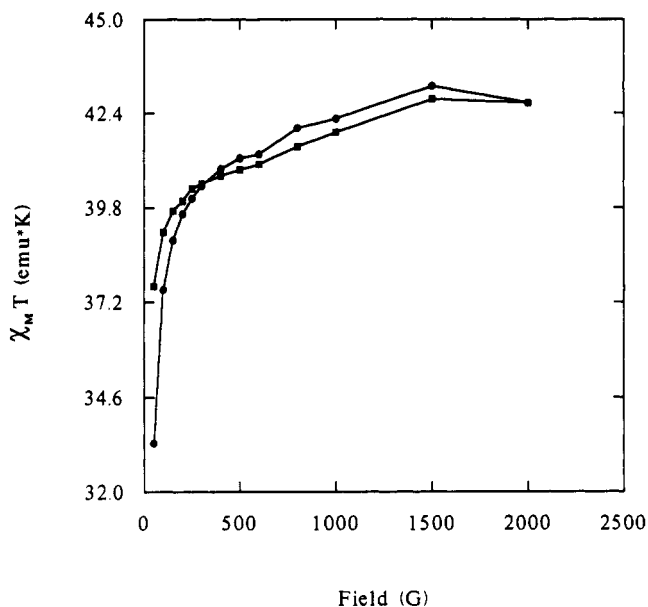


Figure 7. Plot of the molar paramagnetic susceptibility times temperature, $\chi_M T$, versus external magnetic field for a parafilm-embedded polycrystalline sample of $[\text{Mn}_{12}\text{O}_{12}(\text{O}_2\text{CPh})_{16}(\text{H}_2\text{O})_4]$ (3). Data were first measured with increasing field (□) starting at 100 G, and then the field was decreased (○) from 2000 G.

available in the supplementary material. The structure of 3 is depicted in Figure 1, and stereoviews are presented in Figure 2. Inspection of the figures shows that complex 3 can be conveniently described as a central $[\text{Mn}_4\text{O}_4]^{8+}$ cubane held within a nonplanar ring of eight additional manganese atoms by eight $\mu_3\text{-O}$ atoms, $\text{O}(17)\text{-O}(24)$. Peripheral ligation is by sixteen $\mu_2\text{-O}_2\text{CPh}^-$ and four terminal H_2O groups, the latter being oxygen atoms $\text{O}(25)\text{-O}(28)$. All manganese atoms have a distorted octahedral coordination geometry, and the overall molecule approximates to D_2 symmetry. On the basis of Mn-O bond distances, the cubane atoms Mn(1)-Mn(4) are assigned as the four Mn^{IV} centers, and the eight "ring" manganese atoms are assigned as Mn^{III} centers. Octahedral Mn^{III} (d^4) would be expected to show a Jahn-Teller

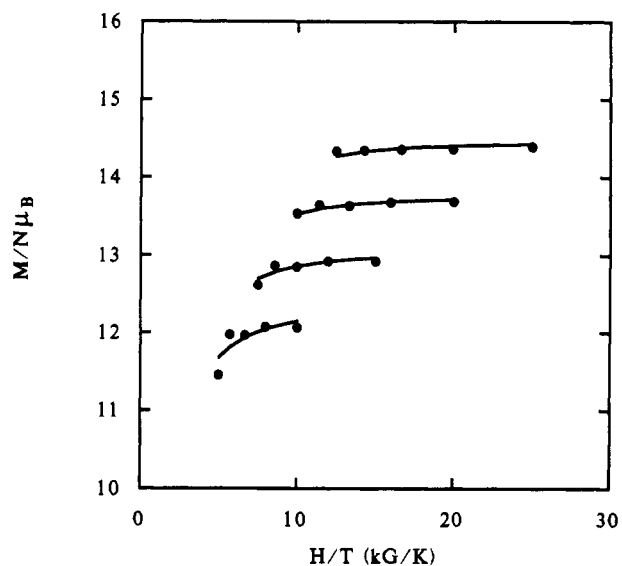
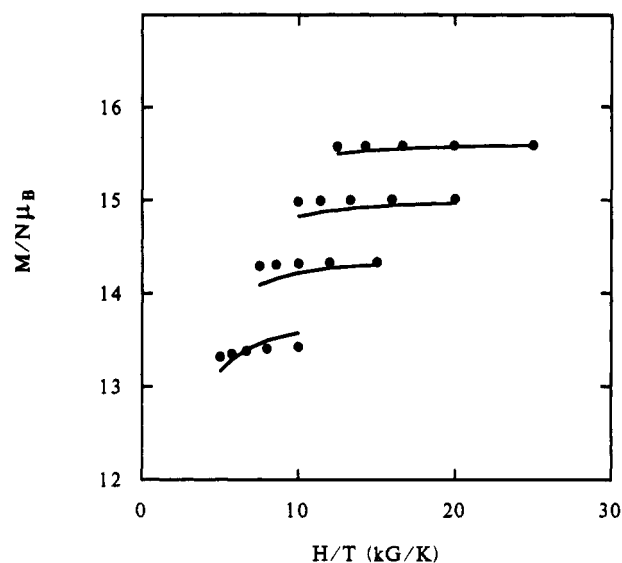


Figure 8. Plots of reduced magnetization, $M/N\mu_B$ (N is Avogadro's number and μ_B is the Bohr magneton), versus H/T for two samples of complex 3. Data were obtained for each compound at 20.0, 30.0, 40.0, and 50.0 kG. The solid lines resulted from least-squares fitting of the data. The upper figure is for a parafilm-embedded polycrystalline sample of the nonsolvated $[\text{Mn}_{12}\text{O}_{12}(\text{O}_2\text{CPh})_{16}(\text{H}_2\text{O})_4]$ (3). The lower figure is for a parafilm-embedded polycrystalline sample of the solvated complex $3\text{-PhCOOH}\cdot\text{CH}_2\text{Cl}_2$.

distortion, and this is apparent in manganese atoms Mn(5-12), each of which has a J-T elongation along the axes approximately parallel to the unique molecular C_2 axis. Consequently, as is evident in Table IV, average axial $\text{Mn}^{\text{III}}\text{-benzoate}$ bond lengths, $\text{Mn}^{\text{III}}\text{-O}_{\text{b,ax}}$, are distinctly longer (2.176 Å) than equatorial lengths, $\text{Mn}^{\text{III}}\text{-O}_{\text{b,eq}}$ (1.955 Å). The four water molecules, two each on Mn(8) and Mn(12), are all on J-T axial sites, and therefore the $\text{Mn}^{\text{III}}\text{-O}_{\text{w}}$ bond lengths (2.214 Å) are similar to $\text{Mn}^{\text{III}}\text{-O}_{\text{b,ax}}$ values. In contrast, the six $\text{Mn}^{\text{IV}}\text{-O}$ distances around each of the central cubane Mn atoms are on average shorter and in a comparatively narrower range, 1.838(20)-1.988(20) Å, the spread being due to the different O atoms involved, benzoate vs bridging O^{2-} . A comparison between $\text{Mn}^{\text{IV}}\text{-O}_{\text{b}}$ (1.919 Å) and $\text{Mn}^{\text{III}}\text{-O}_{\text{b,eq}}$ (1.955 Å) is more appropriate and further supports the cubane Mn atoms to be in the higher oxidation state. As expected, the Mn...Mn separations divide into two distinct types based on the number of bridging oxides (rather than the metal oxidation states). Thus, Mn_2 pairs bridged by one or two oxides have average Mn...Mn separations of >3.3 and <3.0 Å, respectively. The cubane Mn_4 tetrahedron is distorted from pure T_d symmetry to D_{2d} with

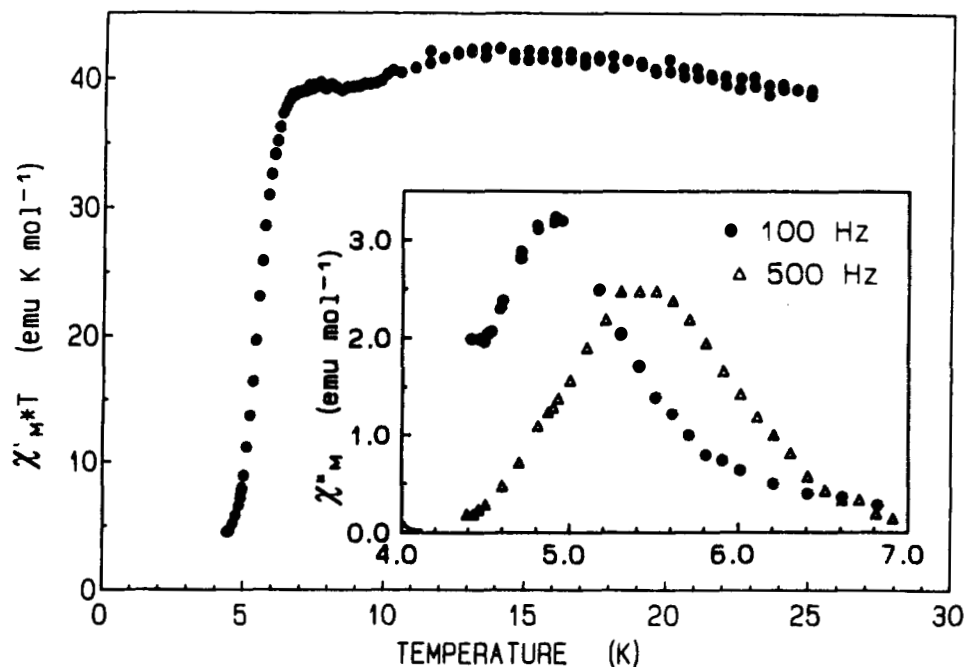


Figure 9. Temperature dependence of $\chi_M'T$ for a polycrystalline sample of $[\text{Mn}_{12}\text{O}_{12}(\text{O}_2\text{CPh})_{16}(\text{H}_2\text{O})_4]$ (3), where $\chi_M'T$ is the real component of the molar magnetic susceptibility measured in a zero applied field with an AC susceptometer. In the inset is shown a plot of the imaginary part of the AC susceptibility, χ_M'' , versus temperature measured at two different frequencies.

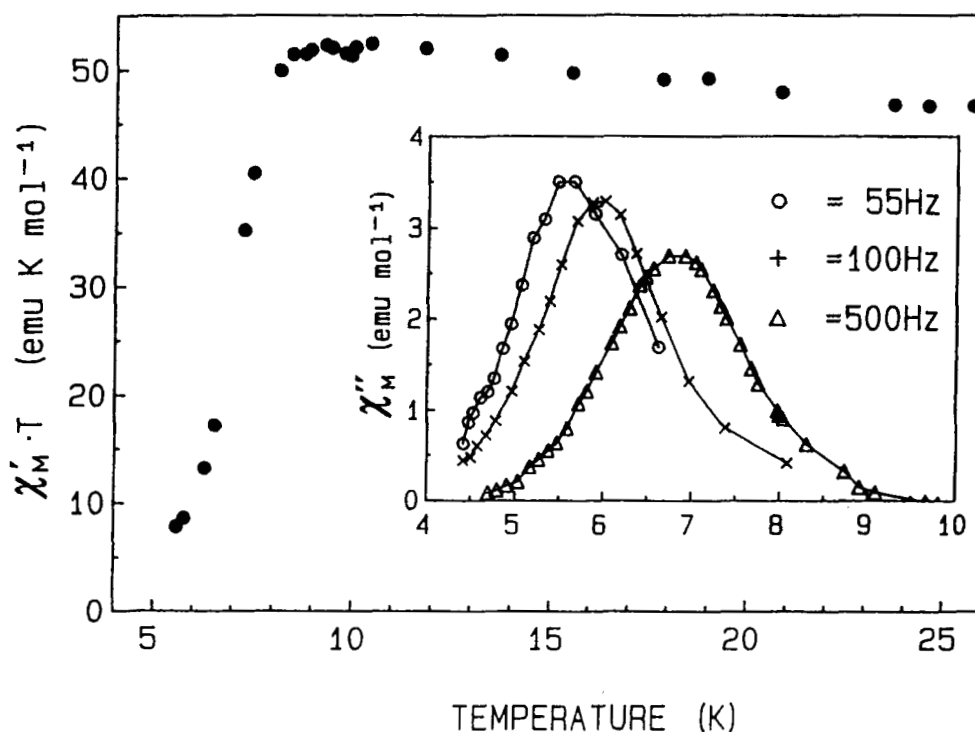


Figure 10. Temperature dependence of $\chi_M'T$ for a polycrystalline sample of $[\text{Mn}_{12}\text{O}_{12}(\text{O}_2\text{CMe})_{16}(\text{H}_2\text{O})_4] \cdot 2\text{MeCO}_2\text{H} \cdot 4\text{H}_2\text{O}$ (4), where χ_M' is the real component of the molar magnetic susceptibility measured in zero applied field with an AC susceptometer. In the inset is shown a plot of the imaginary part of the AC susceptibility, χ_M'' , versus temperature measured at three different frequencies.

equatorial Mn(1)---Mn(3) and Mn(2)---Mn(4) distances (2.981(7) and 3.000(7) Å, respectively) being noticeably longer than the other four (2.820(7)–2.834(7) Å). Overall, the structure of 3 is very similar to that of the acetate analogue, complex 4; however, it is not identical. Complex 4 has imposed S_4 symmetry with one H_2O group on each of *four* Mn atoms (rather than two waters each on two Mn atoms as in complex 3). The two isomeric forms of the $[\text{Mn}_{12}\text{O}_{12}(\text{O}_2\text{CR})_{16}(\text{H}_2\text{O})_4]$ molecule can be interconverted as follows: interchange water oxygen O(27) and benzoate oxygen O(74), and similarly interchange O(25) with O(129). This alters the symmetry from D_2 (3) to S_4 (4).

It is instructive to dissect the structure of complex 3 and to consider the nature of the fragments thus obtained, because many have been previously obtained in discrete form. Shown in Figure 12 are nine smaller nuclearity Mn/O units that can readily be identified with complex 3. Fragments A and B have been seen in numerous dinuclear complexes with a variety of terminal ligands;³² similarly, C is a very common unit, found within the $[\text{Mn}_3\text{O}(\text{O}_2\text{CR})_6\text{L}_3]^{0,+}$ complexes (L = neutral donor group).^{21,33}

(32) A recent tabulation is available: see Que, L., Jr.; True, A. E. *Prog. Inorg. Chem.* 1990, 38, 97.

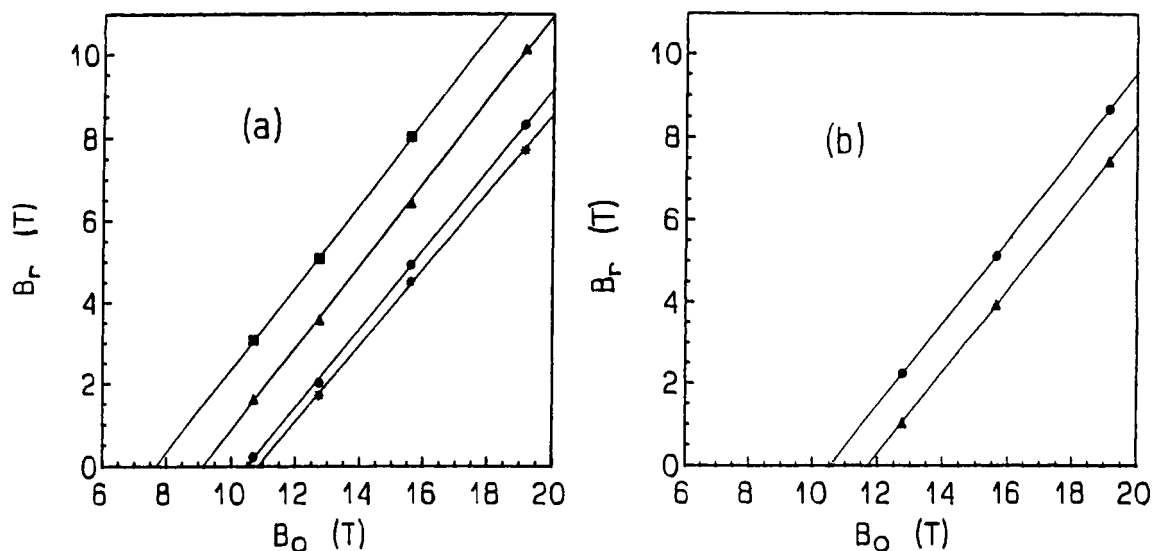


Figure 11. Plots of the resonance fields, B_r , as a function of applied magnetic field, B_0 , obtained from EPR spectra recorded with a high-field spectrometer operating with a CO₂ laser. Plot a is for $[\text{Mn}_{12}\text{O}_{12}(\text{O}_2\text{CMe})_{16}(\text{H}_2\text{O})_4] \cdot 2\text{MeCO}_2\text{H} \cdot 4\text{H}_2\text{O}$ (4), whereas plot b is for $[\text{Mn}_{12}\text{O}_{12}(\text{O}_2\text{CPh})_{16}(\text{H}_2\text{O})_4]$ (3).

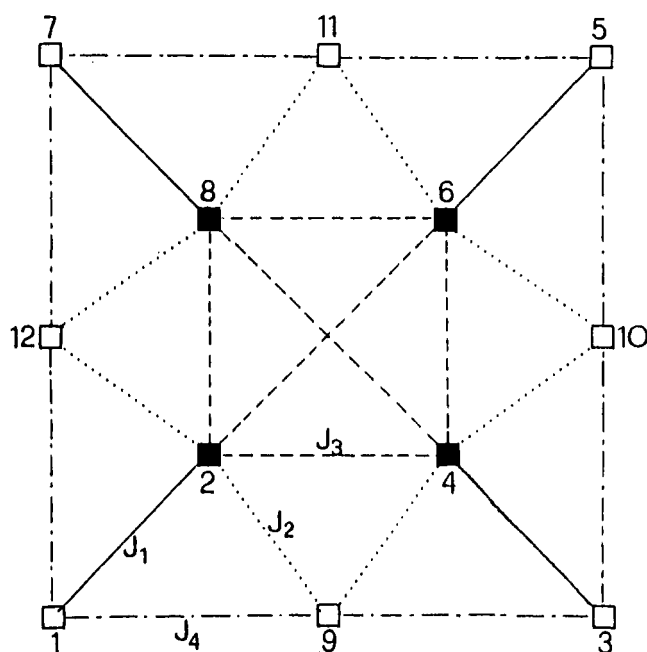
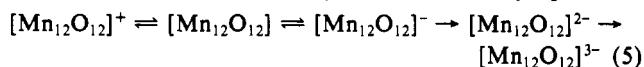


Figure 12. Schematic drawing representing the various pairwise magnetic exchange interactions in a $[\text{Mn}_{12}\text{O}_{12}(\text{O}_2\text{CR})_{16}(\text{H}_2\text{O})_4]$ complex.

Fragment D has only recently been discovered in discrete form, and a handful of examples are now known³⁴ at the Mn_3^{IV} level, not $\text{Mn}^{\text{III}}\text{Mn}_2^{\text{IV}}$ as in 3. Fragment E, a partial cubane and itself a subfragment of cubane I, is currently unknown in discrete form. Fragment H is a common unit in discrete molecules, and many examples are now known that contain the Mn_4O_2 core with either a planar or bent ("butterfly") disposition of the four Mn atoms.^{29-31,35} Indeed, complex 3 can be described as comprising four vertex-sharing butterfly Mn_4O_2 units; one such unit, for

example, is $\text{Mn}(1,5,6,12)\text{O}(17,18)$. Fragments F and G have yet to be discovered in discrete tri- and tetranuclear complexes, respectively, although they are also present as subfragments in other higher-nuclearity species.³⁶⁻³⁸ Finally, Mn_4^{IV} cubane fragment I has yet to be discovered in discrete form, although lower oxidation state ($\leq \text{II}$) forms with bridging OH^- , mixed OH^-/F^- , or OR^- ($\text{R} = \text{alkyl, aryl}$) are known.³⁹ There appears to be no reason why any of the currently unknown fragments E, F, G, and I should not be amenable to synthesis in discrete form. There are, of course, other ways that complex 3 could be dissected to give a number of various nuclearity units of lower symmetry.

Electrochemical Studies. Complexes 3 and 4 have been investigated by cyclic voltammetry (CV) and differential pulse voltammetry (DPV). In Figure 4 are displayed the CV and DPV traces for 3 in CH_2Cl_2 solution. There are several redox couples apparent, three on the reduction side and one on the oxidation side. Two of these redox couples appear to be reversible, the oxidation process at 0.79 V and the first reduction process at 0.11 V. For these two, the forward and reverse waves are well formed with a peak separation (160–170 mV) comparable to that of ferrocene under the same conditions. This also supports their assignment as one-electron processes. The peak separation for the second reduction at -0.23 V is much larger (320 mV), and the third reduction at -0.77 V has little or no reverse wave. Both of these latter reductions thus appear to be electrochemically irreversible, a conclusion supported by the DPV scans that show broader, ill-formed peaks in contrast to the sharper, better-formed peaks for the two reversible couples. Both reversible processes give linear i_p vs $\nu^{1/2}$ plots ($i_p = \text{CV peak current}$) in the scan rate (ν) range 20–500 mV/s, indicating diffusion-controlled processes. The electrochemical results may be summarized by eq 5. The



oxidation and three reductions are presumably centered on the outer ring Mn^{III} and cubane Mn^{IV} atoms, respectively; isolation and structural characterization of both the monoanion and the monocation are objectives for the future to address this point (among others), and initial success in the generation and isolation

(33) Bhula, R.; Gainsford, G. J.; Weatherburn, D. C. *J. Am. Chem. Soc.* **1988**, *110*, 7550.

(34) (a) Auger, N.; Girerd, J.-J.; Corbella, M.; Gleizes, A.; Zimmermann, J.-L. *J. Am. Chem. Soc.* **1990**, *112*, 448. (b) Sarenski, J. E.; Holden, H. H.; Brudvig, G. W.; Crabtree, R. H.; Schulte, C. K. *J. Am. Chem. Soc.* **1990**, *112*, 7255.

(35) (a) Mikuriya, M.; Yamato, Y.; Tokii, T. *Chem. Lett.* **1991**, 1429. (b) Chandra, S. K.; Chakravorty, A. *Inorg. Chem.* **1991**, *30*, 3795. (c) Thorp, H. H.; Sarneshi, J. E.; Kulawiec, R. J.; Brudvig, G. W.; Crabtree, R. H.; Papaefthymiou, G. C. *Inorg. Chem.* **1991**, *30*, 1153. (d) Gedye, C.; Harding, C.; McKee, V.; Nelson, J.; Patterson, J. *J. Chem. Soc., Chem. Commun.* **1992**, 392.

(36) Perlepes, S. P.; Huffman, J. C.; Christou, G. *J. Chem. Soc., Chem. Commun.* **1991**, 23, 1657.

(37) Wang, S.; Huffman, J. C.; Folting, K.; Streib, W. E.; Lobkovsky, E. B.; Christou, G. *Angew. Chem., Int. Ed. Engl.* **1991**, *30*, 1672.

(38) Bhula, R.; Collier, S.; Robinson, W. T.; Weatherburn, D. C. *Inorg. Chem.* **1990**, *29*, 4027.

(39) (a) Herbehold, M.; Wehrmann, F.; Neugebauer, D.; Huttner, G. *J. Organomet. Chem.* **1978**, *152*, 329. (b) Brooker, S.; McKee, V.; Shephard, W. B.; Pannell, L. *J. Chem. Soc., Dalton Trans.* **1987**, 2555. (c) Horn, E.; Snow, M. E.; Zeleny, P. C. *Aust. J. Chem.* **1980**, *33*, 16549.

of $[Mn_{12}O_{12}(O_2CPh)_{16}(H_2O)_4]^-$ (as the NPr_4^{n+} and PPh_4^+ salts) has, in fact, recently been reported.¹⁹

The acetate analogue, complex 4, has only slight solubility in common organic solvents in which it is stable. For example, it will readily dissolve in DMF but soon starts precipitating a fine brown insoluble powder, presumably a manganese oxide. Complex 4 is, however, sufficiently soluble and stable in MeCN to allow electrochemical studies. In Figure 5 are shown the CV and DPV scans for 4 in MeCN (4 is insoluble in CH_2Cl_2 and 3 is insoluble in MeCN, preventing the study of both complexes in the same solvent). The scans are very similar to those for 3, with two reversible features, one oxidation and one reduction. The potentials are essentially identical to those of 3. The electron-transfer series of eq 5 thus also describes the behavior of 4. Attempts to isolate other oxidation states of 4 are in progress.

The $[Mn_{12}O_{12}(O_2CR)_{16}(H_2O)_4]$ complex type is clearly capable of adopting a number of stable oxidation levels, which suggests that it should be feasible to access changes in properties as a function of oxidation state. Initial results along these lines have been reported,¹⁹ and additional work is in progress.

DC Magnetic Susceptibilities. If there were no magnetic exchange interactions present in a $Mn^{IV}Mn^{III}$ complex, the spin-only effective magnetic moment with $g = 2.0$ should be $\mu_{eff} = 15.87 \mu_B$. From Figure 6 it can be seen that μ_{eff}/Mn_{12} for complex 3 at 320 K is $\sim 12 \mu_B$. The main conclusion that can be reached from the 320 K value of μ_{eff}/Mn_{12} is that there are appreciable exchange interactions present. Not all of the spin states of the Mn_{12} complex are thermally populated. The increase in $\mu_{eff}/molecule$ with decreasing temperature (Figure 6) observed for complex 3 was also seen²² for complex 4. This behavior may reflect some ferromagnetic coupling in the Mn_{12} complexes. However, it is more likely that this increase reflects the fact that as the temperature is decreased, only one (or a few) state(s) is (are) populated.

In Figure 6 are shown plots of $\mu_{eff}/molecule$ versus temperature for several different samples of complex 3. All of these data were collected at 10.0 kG. In addition to the data in Figure 6, similar 10.0-kG data were obtained for eight other samples of complex 3. Data were collected for unrestrained polycrystalline samples, both nonpowdered and powdered, for polycrystalline samples milled in petroleum jelly, and for polycrystalline samples pressed into a sheet of parafilm. The variability in $\mu_{eff}/molecule$ versus temperature plots for the various samples reflects three basic facts. First, apparently polycrystalline samples of these Mn_{12} complexes have considerable magnetic anisotropy (vide infra), for we have found that even in fields as small as ~ 1 kG there is evidence of torquing in the crystallites. Second, there are two crystallographically different forms of complex 3, and the $\mu_{eff}/molecule$ versus temperature curves are somewhat different between the two forms. One form ($P\bar{I}$) has been characterized by X-ray crystallography to be a nonsolvated form of complex 3. The other form is a solvate with one molecule of benzoic acid and one CH_2Cl_2 , i.e., $3 \cdot PhCOOH \cdot CH_2Cl_2$. Preliminary single-crystal X-ray work indicates that this second form is different from the other form. Third, when the petroleum jelly mulling technique is employed to avoid torquing of the polycrystallites in a magnetic field, it is difficult to determine an accurate value for the mass of the sample.

In our previous communication,¹⁷ it was concluded that nonsolvated complex 3 has a $S = 14$ ground state. This conclusion is in error. Reduced magnetization, $M/N\mu_B$ (N is Avogadro's number and μ_B is the Bohr magneton) versus H/T data were measured at 48.0, 30.0, and 10.0 kG in the 1.63–20 K range for a ~ 3 -mg sample of complex 3 milled in petroleum jelly. Least-squares fitting of these data, where the spin Hamiltonian matrix was diagonalized on each iteration, was used to conclude that nonsolvated complex 3 has a $S = 14$ ground state. There is no problem with crystallites torquing in an external field when they are milled in petroleum jelly. The inaccuracy in this measurement enters when it becomes necessary to determine the mass of the ~ 3 -mg sample milled in petroleum jelly. This was done previously¹⁷ by a comparison of data for the petroleum

jelly-mulled sample at 10.0 kG to data for the unrestrained polycrystalline sample at 10.0 kG in the 4.2–20 K range. Through careful measurements on many different samples (vide infra), we now know that this approach to determining the sample mass for this highly magnetically anisotropic material is not very accurate. It was assumed¹⁷ that there was little torquing of complex 3 in a 10.0-kG field. After carrying out susceptibility measurements on several samples of complex 3 under a variety of conditions, we have found that a good way to avoid torquing of a polycrystalline sample in a magnetic field is to embed a powder in a parafilm sheet. A small sample (~ 10 – 20 mg) of very small crystallites is spread on a parafilm sheet which is then folded over several times. Pressure on the parafilm "pill" embeds the crystallites in the film and minimizes torquing. In Figure 6 are shown plots of $\mu_{eff}/molecule$ versus temperature at 10.0 kG for an unrestrained polycrystallite sample (\bullet) as well as two different (∇ and \blacktriangledown) parafilm-embedded samples of the nonsolvated complex 3. In agreement with our previous communication,¹⁷ there is a maximum in $\mu_{eff}/molecule$ of $23.6 \mu_B$ at 11 K for the unrestrained sample. However, the maximum value of $\mu_{eff}/molecule$ for the parafilm-embedded samples is found at the smaller value of $\sim 20.8 \mu_B$ at ~ 20 K. It can also be seen that the $\mu_{eff}/molecule$ versus temperature curve is steeper for the unrestrained sample, a possible signature of partial torquing of crystallites in the 10.0 kG field.

Variable-temperature susceptibility data were also run for a parafilm-embedded sample of the solvated complex $3 \cdot PhCOOH \cdot CH_2Cl_2$. Data for two samples (\square and \blacksquare) are shown. The $\mu_{eff}/molecule$ versus temperature data for this solvated complex are somewhat different than those for the nonsolvated complex, see Figure 6. The maximum in $\mu_{eff}/molecule$ occurs at the smaller value of $\sim 19.8 \mu_B$ at 15 K.

A parafilm-embedded polycrystalline sample of $[Mn_{12}O_{12}(O_2CPh)_{16}(H_2O)_4]$ (3) was examined for hysteresis effects. In Figure 7 is shown a plot of $\chi_M T$ versus applied magnetic field. The sample was first introduced into the SQUID susceptometer with the field off, and then the field was set at 100 G. The field was increased in increments up to 2000 G, with 4 min being taken to make a susceptibility measurement at each field. The field was then decreased in increments. As can be seen, at fields above ~ 300 G as the field was decreased in increments, the value of $\chi_M T$ was found to be greater than the corresponding value measured with increasing field. Some small hysteresis is indicated. However, below ~ 300 G the value of $\chi_M T$ measured with decreasing field falls below the corresponding value measured with increasing field. We attribute this latter effect to the fact that at these low magnetic fields there is some residual field left in the SQUID susceptometer which can only be removed by cycling this high-field SQUID through zero field.

As far as the pairwise magnetic exchange interactions between metal ions are concerned, it is possible to represent complexes 3 and 4 as shown in Figure 12. There are at least four different types of pairwise exchange interactions, to each of which an isotropic exchange parameter (J_{ij} in the spin Hamiltonian $H = 2J_{ij}S_i \cdot S_j$) can be associated. The parameter J_1 refers to $Mn^{IV} \cdots Mn^{III}$ pairs bridged by two μ -oxo ions; J_2 to $Mn^{IV} \cdots Mn^{III}$ pairs bridged by one μ -oxo ion; J_3 to $Mn^{IV} \cdots Mn^{IV}$ pairs; and J_4 to $Mn^{III} \cdots Mn^{III}$ pairs. It is clear from Figure 12 that there are many triangulated arrangements of metal ions which affect the exchange interactions in these complexes. Appreciable spin frustration effects can be anticipated. The calculation of the energy levels of such a $Mn_4^{IV}Mn_8^{III}$ complex can, in principle, be performed with the spin Hamiltonian given in eq 6:

$$H = -2J_1(S_1 \cdot S_2 + S_3 \cdot S_4 + S_5 \cdot S_6 + S_7 \cdot S_8) - 2J_2(S_2 \cdot S_9 + S_4 \cdot S_9 + S_4 \cdot S_{10} + S_6 \cdot S_{10} + S_6 \cdot S_{11} + S_8 \cdot S_{11} + S_8 \cdot S_{12} + S_2 \cdot S_{12}) - 2J_3(S_2 \cdot S_4 + S_2 \cdot S_6 + S_2 \cdot S_8 + S_4 \cdot S_6 + S_4 \cdot S_8 + S_6 \cdot S_8) - 2J_4(S_1 \cdot S_9 + S_1 \cdot S_{12} + S_8 \cdot S_9 + S_3 \cdot S_{10} + S_5 \cdot S_{10} + S_5 \cdot S_{11} + S_7 \cdot S_{11} + S_7 \cdot S_{12}) \quad (6)$$

For a $Mn_4^{IV}Mn_8^{III}$ complex, the dimension of the full spin Hamiltonian matrix is prohibitively large, $10^8 \times 10^8$. If the spin of the states is used to block this matrix, the matrix can be factored

into 23 blocks for spin values ranging from $S = 0$ to $S = 22$. The largest block is of the dimensions of $(1\ 111\ 696) \times (1\ 111\ 696)$.

It is important to note that even though we tried many coupling schemes, it is impossible to use the Kambe vector coupling scheme⁴⁰ to simplify eq 6. Depending on the topology and connectivity in a cluster, in several cases it is possible to define a coupling scheme such that all of the $S_i S_j$ operator terms in eq 6 can be replaced by S_i^2 operators. If this were possible, then eq 6 could be replaced by an equation giving directly the eigenvalues of all the spin states. This is not possible for complexes 3 and 4.

Even though quantitative descriptions of the entire spin manifolds of complexes 3 and 4 are not yet possible, the nature of the ground state can be determined by examining the magnetization of the compound at low temperatures as a function of applied magnetic field. Figure 8 (upper) shows four isofield plots of $M/N\mu_B$ versus H/T determined for a parafilm-embedded polycrystalline sample of the nonsolvated complex 3, i.e., $[\text{Mn}_{12}\text{O}_{12}(\text{O}_2\text{CPh})_{16}(\text{H}_2\text{O})_4]$. At 50 kG and 2.00 K, the value of $M/N\mu_B$ is 15.6. It can be seen that the data sets measured at 40.0, 30.0, and 20.0 kG do not plateau at the same value as for the 50.0-kG data set. If there is only one state populated at these low temperatures in these applied fields, then the nonsuperimposability of the five isofield data sets indicates that the ground state has appreciable zero-field splitting.

The magnetization for such a complex may be calculated by using the basic thermodynamic relation⁴¹ given in eq 7. This

$$M = N \sum_{i=1}^P \left(\frac{-\delta E_i}{\delta H} \right) \exp(-E_i/kT) / \sum_{i=1}^P \exp(-E_i/kT) \quad (7)$$

equation reduces to the Brillouin function in the case of no zero-field splitting. In eq 7, N is Avogadro's number, and $\delta E_i/\delta H$ is the change in the energy of the i th level in response to a change in a magnetic field. The energies of the various spin sublevels are obtained by diagonalization of the spin Hamiltonian matrix, including the Zeeman terms.

The solid lines in Figure 8 (upper) represent a least-squares fit of all of the four isofield magnetization data sets for the parafilm-embedded sample of $[\text{Mn}_{12}\text{O}_{12}(\text{O}_2\text{CPh})_{16}(\text{H}_2\text{O})_4]$ (3). The spin of the ground state was taken as $S = 10$, and the least-squares fitting parameters were found to be $g = 1.93$ and $D = 0.50\text{ cm}^{-1}$ with TIP held fixed at 2400×10^{-6} cgsu. The parameter D characterizes the axial ($D\hat{S}_z^2$) zero-field splitting in the $S = 10$ ground state. If the ground state was assumed to have $S = 9$, then a g value of 2.55 was obtained; for $S = 11$, a g value of 1.75 was obtained. These g values are not as reasonable as the $g = 1.93$ value obtained for $S = 10$. Thus, if there is only one state populated at temperatures of 2.0–4.0 K, then the ground state of the nonsolvated complex $[\text{Mn}_{12}\text{O}_{12}(\text{O}_2\text{CPh})_{16}(\text{H}_2\text{O})_4]$ (3) in an external field is the $M_S = -10$ component of the $S = 10$ state.

In the lower part of Figure 8 are shown plots of $M/N\mu_B$ versus H/T for a parafilm-embedded sample of the solvated complex $[\text{Mn}_{12}\text{O}_{12}(\text{O}_2\text{CPh})_{16}(\text{H}_2\text{O})_4] \cdot \text{PhCOOH} \cdot \text{CH}_2\text{Cl}_2$. These data were measured at fields of 50.0, 40.0, 30.0, and 20.0 kG and in each case in the range of 2.0–4.0 K. It can be seen that the data for this solvated form of complex 3 are similar to those for the nonsolvated form, except all of the isofield data sets for the solvated complex fall at smaller values. The data for the solvated complex fit best with $S = 9$ with the parameters $g = 1.86$ and $D = 0.40\text{ cm}^{-1}$. It is possible there is a small difference in the spin value of the ground state of these two different forms of complex 3. The sample history dependence of the susceptibility data and the X-ray structure of the solvated form will have to be determined before we can decide whether the two forms do, indeed, have different spin ground states.

Caneschi et al.¹⁸ reported the results of isothermal magnetization measurements for complex 4 carried out in the 4.2–60 K range with external fields of 20, 120, and 200 kG. The magnetization

readily saturates for H/T greater than 1 T/K at the value expected for $S = 10$. Thus, the three isothermal magnetization versus H/T plots were found to be nearly superimposable. It was concluded that complex 4 has a $S = 10$ ground state both in an external field and with a zero external field.

AC Magnetic Susceptibilities. The AC susceptibility data measured in the earth's magnetic field for complexes 3 (nonsolvated) and 4 (Figures 9 and 10, respectively) are fascinating. Two types of information can be extracted. From the plateaus in the $\chi'_M T$ (χ'_M is the real part of AC susceptibility) versus temperature data it is possible to characterize the ground state in zero applied field. For the acetate complex 4 the product $\chi'_M T$ reaches a plateau at $52.3\text{ emu K mol}^{-1}$ ($\mu_{\text{eff}} = 20.4\ \mu_B$). This is consistent with a $S = 10$ ground state where $g = 1.9$, which was also found¹⁸ from the high-field magnetization data for complex 4. From 5 to 24 K the value of $\chi'_M T$ for complex 3 is essentially constant at $\sim 41\text{ emu K mol}^{-1}$ ($\mu_{\text{eff}} = 17.2\ \mu_B$). This indicates that complex 3 at zero applied field has a $S = 9$ ground state with $g \approx 1.9$.

The second type of information readily obtainable from the AC susceptibility data for both complexes 3 and 4 is that there are relaxation effects associated with the magnetization. The relatively abrupt decrease in $\chi'_M T$ at low temperatures is the first indication of the onset of relaxation effects. Conclusive evidence of relaxation effects can be drawn from the fact that there is a nonzero imaginary component of the susceptibility, χ''_M . Furthermore, measurements performed at various frequencies show that for both complexes the temperature at which the maximum in χ''_M occurs is frequency dependent. In the AC susceptibility experiment the external magnetic field is being reversed at some frequency (e.g., 55–500 Hz). The magnetization of the sample responds to this oscillating external magnetic field. In the case of a simple paramagnet the magnetization of the sample can relax very rapidly (nanoseconds), and it can follow the oscillating external field. No out-of-phase component (imaginary part) of the AC susceptibility is expected. If the sample's magnetization relaxes (responds) slowly, then there is a nonzero imaginary component. Such is the case for a magnetic material which has large enough crystallites that they are multidomain crystallites.

A paramagnet can show relaxation effects in the presence of an external magnetic field. Our experiments were performed without shielding the earth's magnetic field ($\sim 0.5\text{ G}$), but even in the presence of such a high magnetic anisotropy it seems highly unlikely that the earth's magnetic field would induce relaxation effects for a simple paramagnet.

Relaxation effects in zero applied field can be observed in materials with a spontaneous magnetization at the critical temperature, but in this case the temperature at which the maxima are observed should not be frequency dependent. Frequency-dependent maxima have been observed for superparamagnets⁴² and spin glasses.⁴³ The former are ferromagnetic materials composed of small particles in which the magnetization competes with thermal agitation. The presence of shape anisotropy and/or magneto crystalline anisotropy determines a barrier, W , to reorientation between two possible opposite easy axis directions. A relaxation time τ can be defined:

$$\tau = \tau_0 \exp(-W/Kt) \quad (8)$$

When $\tau \approx 1/\nu_m$, where ν_m is the operating frequency of the AC susceptometer, the system cannot reorient and relaxation effects become apparent. The blocking temperature is frequency dependent. In our case we have large spins, but it is not easy to imagine that the clusters can be considered as superparamagnetic particles. In fact, we have investigated other clusters (e.g., $[\text{Mn}_6^{II}(\text{nitroxide})_6]^{16}$ with a ground $S = 12$ state) which do not show any relaxation effects in zero applied field.

A spin glass is an assembly of spins which have random mixed interactions. Mixed interactions are certainly present in the Mn_{12}

(40) Kambe, K. *J. Phys. Soc. Jpn.* 1950, 5, 48.

(41) Vermaas, A.; Groeneveld, W. L. *Chem. Phys. Lett.* 1984, 27, 583.

(42) Richardson, J. T.; Milligan, W. D. *Phys. Rev. B* 1956, 102, 1289.

(43) Nagata, S.; Keesom, P. H.; Harrison, H. N. *Phys. Rev. B* 1979, 19, 1363.

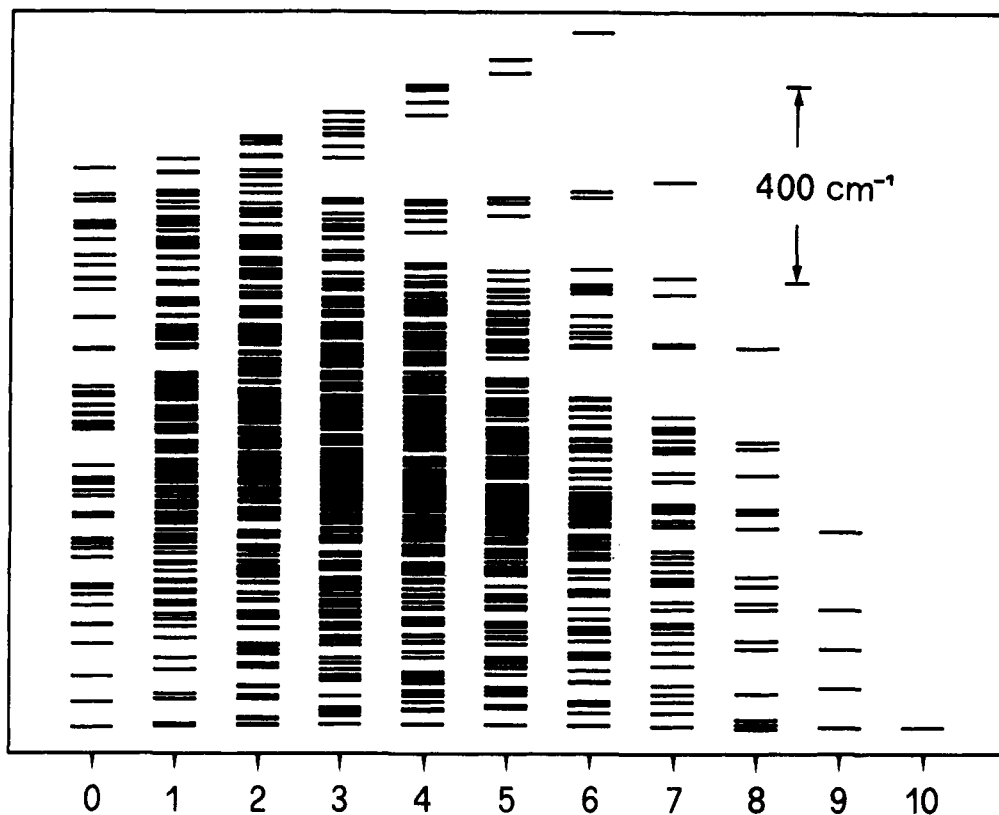


Figure 13. Calculated energies of the spin states of a $Mn^{IV}_4Mn^{III}_8$ complex assuming $J_2 = -60 \text{ cm}^{-1}$ and $J_3 = -60 \text{ cm}^{-1}$. See the text for a discussion of the theoretical model.

clusters where frustration effects are operative, but randomness is not easily reconciled with the crystalline nature of the compounds.

High-Field EPR Spectroscopy. The EPR spectra of complexes 3 and 4 indicate the presence of two low-lying levels within which transitions can be excited by the far infrared laser. Their frequency dependence clearly shows that these levels are split in zero field by ca. 10 cm^{-1} . Further, since only low-field transitions are observed, the sign of the zero field splitting must be such that $D < 0$, i.e., the states with large M_S are lowest in energy. This gives rise to a very large anisotropy. In fact, if we assume that for complex 4 the ground state can be described as $S = 10$, then the axial zero field splitting establishes the $M_S = \pm 10$ level as lowest in energy. The first excited level has $M_S = \pm 9$ and is separated from the $M_S = \pm 10$ level by 19 D in energy. The EPR spectra therefore suggest $D \approx -0.6 \text{ cm}^{-1}$. The energies of the lowest two states in our external field are $\pm 10 g'' \mu_B B$ in a field parallel to the tetragonal axis, while in a field orthogonal to the axis the two levels are not split in first approximation (in a small field). Therefore, in a moderate field the molecules in the ground state have a large magnetic anisotropy and strong orientation effects can be observed.

The above D value is somewhat larger than the D value evaluated by fitting the $M/N\mu_B$ versus H/T data for complex 3. This could be due to the fact that D values obtained from fitting bulk susceptibility data are not very accurately determined. In fact, in many cases it is not possible to uniquely determine even the sign of the D value by fitting bulk magnetic susceptibility data.

Theoretical Calculations of Spin-State Orderings. Examination of the data reported⁴⁴ in the literature for $Mn^{III}\dots Mn^{III}$, $Mn^{IV}\dots Mn^{III}$, and $Mn^{IV}\dots Mn^{IV}$ magnetic exchange interactions suggests that J_1 should be larger than the other three J values. Typical values are $J_1 \approx -150 \text{ cm}^{-1}$. The J_4 type of interaction has always

been found to be weak, either ferromagnetic or antiferromagnetic with $|J_4| \leq 30 \text{ cm}^{-1}$. The J_2 and J_3 types of interactions are generally antiferromagnetic and presumably not too different from each other.

If we assume that J_1 is antiferromagnetic and larger than all the others, it is likely that the ground state must belong to a configuration in which all the $Mn^{III}\dots Mn^{IV}$ pairs connected by bis- μ -oxo bridges are paired up to give $S = 1/2$ units. In this way we have to take into account only four $S = 1/2$ units and four $S = 2$ Mn^{III} ions. The allowed spin states range from 0 to 10, and the maximum dimensions become 248×248 for the $S = 3$ block of the spin Hamiltonian matrix. In this way the problem becomes tractable. Some of the present authors²⁷ have introduced an efficient procedure for the calculation of the energy levels of clusters which can work on this size of a problem. Of course, this simplified model cannot be expected to provide a good description of the susceptibility of the cluster at high temperature, but it can be hoped that it is accurate enough for the low lying levels.

Sample calculations were performed by varying J_2 and J_3 while keeping $J_4 = 0$. The low-lying energy levels are very close to each other, and minor variations of J_2 and J_3 can drastically alter the nature of the ground state. For instance, for $J_2 = -60 \text{ cm}^{-1}$ and $J_3 = -60 \text{ cm}^{-1}$ (case 1), the ground state is $S = 8$ with two $S = 9$ states and one $S = 10$ state at 4.3 cm^{-1} and a $S = 0$ state at 4.5 cm^{-1} . For $J_2 = -60 \text{ cm}^{-1}$ and $J_3 = -62.5 \text{ cm}^{-1}$ (case 2), the ground state becomes $S = 0$ with a $S = 8$ state at 0.9 cm^{-1} . For $J_2 = -60 \text{ cm}^{-1}$ and $J_3 = -57.5 \text{ cm}^{-1}$ (case 3), the ground state is $S = 10$ with a $S = 8$ state at 1.8 cm^{-1} and two $S = 9$ states at 3.3 cm^{-1} . These results are in agreement with the expectations of strong spin frustration effects associated with the exchange topology in these materials.

In order to have a visualization of the complicated density of spin states of these clusters, we plot the energies of the levels of one of the above calculations in Figure 13. The levels are spread in a range of ca. 2800 cm^{-1} , and they are almost continuous.

We did not attempt to fit the experimental data for either complex 3 or 4 due to the approximations inherent in our model; however, we found it extremely rewarding that only minor changes

(44) Tabulated in Hendrickson, D. N.; Christou, G.; Schmitt, E. A.; Libby, E.; Baskin, J. S.; Wang, S.; Tsai, H.-L.; Vincent, J. B.; Boyd, P. D. W.; Huffman, J. C.; Folting, K.; Li, Q.; Streib, W. E. *J. Am. Chem. Soc.* 1992, 114, 2455.

in the magnetic exchange parameters can determine large variations in the ground states and, therefore, the limiting values of the effective magnetic moments at low temperature. Thus, these simplified calculations have satisfactorily shown that with reasonable values of the parameters, close proximity of excited levels of different spin multiplicity is possible.

In the calculations, we have assumed tetragonal symmetry and T_d symmetry as far as the $Mn^{IV} \cdots Mn^{IV}$ interactions are concerned. While complex 4 is, indeed, tetragonal in the crystal, complex 3 is not, so differences in the ground states between the two could be expected.

Concluding Comments

The preparation and X-ray structure of the new $Mn^{IV}_4Mn^{III}_8$ complex, $[Mn_{12}O_{12}(O_2CPh)_{16}(H_2O)_4]$ (3), are reported. It is shown that this new complex and the analogous complex $[Mn_{12}O_{12}(O_2CCH)_{16}(H_2O)_4] \cdot MeCOOH \cdot 4H_2O$ (4) have interesting properties. Complex 4 has a $S = 10$ ground state both in zero applied fields as well as in large (20 T) magnetic fields. The nonsolvated complex 3 appears to have a $S = 9$ ground state in zero applied field, but with the introduction of a magnetic field the ground state becomes the $M_S = -10$ component of a $S = 10$

state.

High-field EPR experiments with a CO_2 laser spectrometer show that there are appreciable zero-field interactions for both of the complexes. High magnetic anisotropy is present.

Perhaps the most interesting observation made for the complexes 3 and 4 is the presence of a nonzero imaginary component of the AC susceptibility. Thus, even though we are dealing with $Mn^{IV}_4Mn^{III}_8$ molecular species, there are magnetization relaxation effects seen in zero applied field. The origin of this relaxation is not clear. Either these complexes are large enough to exhibit relaxation effects, or there are as yet uncharacterized intermolecular interactions present in these solids. Considerable additional experiments are needed to identify the origin of these unusual relaxation effects.

Acknowledgment. This work was partially supported by NSF grants CHE-8808019 (G.C.) and CHE-9115286 (D.N.H.).

Supplementary Material Available: Complete listings of bond lengths and angles, positional parameters, and tables of magnetic susceptibility data for complex 3 (22 pages). Ordering information is given on any current masthead page.

Photochemistry of Intercalated Methylene Blue: Photoinduced Hydrogen Atom Abstraction from Guanine and Adenine

Stephen J. Atherton and Anthony Harriman*

Contribution from the Center for Fast Kinetics Research, The University of Texas at Austin, Austin, Texas 78712. Received July 28, 1992

Abstract: Methylene blue intercalates more effectively into poly[dGdC] ($K = (1.6 \pm 0.4) \times 10^6 M^{-1}$) than poly[dAdT] ($K = (1.6 \pm 0.5) \times 10^4 M^{-1}$); in the latter case, intercalation competes with surface binding ($K = (2.3 \pm 0.6) \times 10^4 M^{-1}$). Intercalation is accompanied by a dramatic reduction in the lifetime of the first excited singlet state, causing decreases in quantum yields for both fluorescence and formation of the triplet state. In the case of methylene blue intercalated into poly[dGdC], transient absorption spectroscopic measurements have shown that the excited singlet state of the dye abstracts a hydrogen atom (or an electron) from an adjacent nucleic acid base, presumed to be guanine on thermodynamic grounds. The rate constants for forward and reverse transfers, respectively, are $(2.5 \pm 0.3) \times 10^{11}$ and $(3.3 \pm 0.4) \times 10^{10} s^{-1}$. The rate constant for the forward transfer in poly[dAdT] is $(1.4 \pm 0.5) \times 10^{10} s^{-1}$ and is presumed to be slower than that of the reverse transfer. Using thermodynamic arguments, it is concluded that the quenching processes involve hydrogen atom transfer from guanine or adenine to the excited singlet state of methylene blue.

The fluorescence of certain polycyclic cationic dyes is quenched upon intercalation between base pairs in polynucleotides such as DNA.¹ Recent studies²⁻⁴ carried out with N,N' -diazapyrenium and N,N' -diazaperopyrenium dyes intercalated into synthetic and natural polynucleotides have provided clear spectroscopic evidence⁴ indicating that fluorescence quenching is due to rapid electron abstraction from an adjacent nucleic acid base by the excited singlet state of the dye. Related studies have reported^{5,6} that the excited singlet state of intercalated methylene blue abstracts an

electron from one of the bases in poly[dGdC], on a time scale of a few picoseconds,⁶ but not from poly[dAdT]. This high specificity is surprising in view of the fact that the one-electron oxidation potentials⁷ of guanine and adenine differ by only 100 mV. Furthermore, the dramatic reduction in excited singlet state lifetime that occurs upon binding to poly[dGdC] is matched by only modest reductions in the quantum yields for fluorescence and for formation of the triplet excited state.⁸ Other workers,⁹ however, have reported that both quantum yields are lowered upon binding to poly[dGdC] and that, due to steric and polarity effects, methylene blue binds more effectively to poly[dGdC] than to poly[dAdT].⁹⁻¹¹

Because so little is known about the dynamics of electron-transfer processes involving polynucleotide matrices,^{4,12} we have

(1) (a) Tubbs, K. R.; Ditmars, W. E.; van Winkler, Q. *J. Mol. Biol.* **1964**, *9*, 545. (b) Kubota, Y.; Fujisaki, Y. *Bull. Chem. Soc. Jpn.* **1977**, *50*, 297. (c) Georgiou, S. *Photochem. Photobiol.* **1977**, *26*, 59.

(2) (a) Blacker, A. J.; Jazwinski, J.; Lehn, J.-M.; Wilhelm, F. X. *J. Chem. Soc., Chem. Commun.* **1986**, 1035. (b) Slama-Schwok, A.; Jazwinski, J.; Bere, A.; Monteny-Garestier, T.; Rougée, M.; Hélène, C.; Lehn, J.-M. *Biochemistry* **1989**, *28*, 3227.

(3) Slama-Schwok, A.; Rougée, M.; Ibanez, V.; Geacintov, N. E.; Monteny-Garestier, T.; Lehn, J.-M.; Hélène, C. *Biochemistry* **1989**, *28*, 3234.

(4) Brun, A. M.; Harriman, A. *J. Am. Chem. Soc.* **1991**, *113*, 8153.

(5) Loeber, G.; Kittler, L. *Stud. Biophys.* **1978**, *73*, 25.

(6) (a) Beddard, G. S.; Kelly, J. M.; van der Putten, W. J. M. *J. Chem. Soc., Chem. Commun.* **1990**, 1346. (b) Kelly, J. M.; Tuite, E. M.; van der Putten, W. J. M.; Beddard, G. S.; Reid, G. D. In *Supramolecular Chemistry*; Balzani, V., De Cola, L., Eds.; NATO ASI Series C, 371; Kluwer: Dordrecht, 1992; p 375.

(7) (a) Kittler, L.; Loeber, G.; Gollmick, F. A.; Berg, M. *J. Electroanal. Chem.* **1980**, *116*, 503. (b) Jovanovic, S. V.; Simic, M. G. *J. Phys. Chem.* **1986**, *90*, 974.

(8) Kelly, J. M.; van der Putten, W. J. M.; McConnell, D. J. *Photochem. Photobiol.* **1987**, *49*, 167.

(9) Hogan, M.; LeGrange, J.; Austin, B. *Nature* **1963**, *304*, 752.

(10) Muller, W.; Crothers, D. M. *Eur. J. Biochem.* **1975**, *54*, 267.

(11) Muller, W.; Bunemann, H.; DattaDupta N. *Eur. J. Biochem.* **1975**, *54*, 279.